Arab J Sci Eng
DOI 10.1007/s13369-016-2138-y

REVIEW ARTICLE – EARTH SCIENCES

Permeability from Microscopy: Review of a Dream

Gabor Korvin[1]

Received: 21 January 2016 / Accepted: 5 April 2016

Abstract The Kozeny–Carman and Timur-type equations connecting porosity and permeability contain rock-textural constants such as tortuosity and specific surface area. Sometimes these are combined in single factors as *Kozeny constant* or *flow zone index*. The partial differential equations of flow in triple-porosity rocks contain *transfer factors*, *interporosity flow shape factors* between different kinds of pores, as well as their individual *storativities*. Without knowing these constants, no meaningful permeability prediction or flow simulation is possible. The paper reviews the main ideas of how to find such rock-textural properties directly from the microscopic image.

Keywords Porosity · Permeability · Tortuosity · Specific surface area · Flow zone index · Kozeny–Carman equation · Timur equation · Monte Carlo

1 Introduction

This Review is about the dream of every petrophysicists to find the rock-textural constants occurring in permeability theory (specific surface area, tortuosity, flow zone index, transfer factors) directly from the always available, informative and digitally treatable optical or SEM rock images. After general questions (thresholding, method of moments, scaling of tortuosity) I shall discuss in details the different approaches proposed in the last five decades for finding rock-textural constants, and ultimately permeability, directly from the rock image. Two basic approaches, based on the Kozeny–Carman (KC) [1] and the Timur's [2,3] equations, will be dealt with. A separate part (Sect. 5) of the Review is devoted to triple porosity, and to the autocorrelation function (ACF) technique of permeability prediction from rock image (Sect. 6). Because of the nature of the topic, mathematics will be fully described and some theorems of probabilistic geometry will be heuristically proved. Wherever appropriate, Monte Carlo algorithms will be recommended and described for estimating otherwise intractable quantities.

1.1 Caveat

The Review only covers permeability estimation from planar microscopic rock images through the KC or Timur-type equations, even though the pore space extends to the 3D space and not confined to the image's plane. Also, the reservoir properties of sedimentary rocks are anisotropic, with their permeability often being much greater in directions parallel to their bedding than in other directions. The solution to these two problems had been at first to use a series of closeby parallel images, as well as using parallel sections of the rock cut in different directions. These experiments have led to the exciting and promising recent development, Digital Rock Physics (DRP) [4,5], what is outside the scope of this paper. In DRP, one reconstructs the 3D pore space of a small ($<1\,\mathrm{cm}^3$) rock cutting by computerized X-ray tomography, digitizes the pore space and then numerically simulates the relevant physical process to get the macroscopic rock properties such as electric resistivity and Archie's exponents, permeability, elastic moduli, etc. Readers interested in DRP applications for permeability are referred to [4–12], ([7] is one of the few studies which seriously addresses the *statistical relevance* of the obtained quantities!).

✉ Gabor Korvin
gabor@kfupm.edu.sa

1 Department of Geosciences and Reservoir Characterization Research Group, King Fahd University of Petroleum and Minerals, Dhahran 31261, Saudi Arabia

Journal: **13369** MS: **2138** ☐ TYPESET ☐ DISK ☐ LE ☐ CP Disp.:**2016/4/13** Pages: **21** Layout: **Large**

Another aspect deliberately neglected in the review is how to find the various kinds of fractal dimensions of the pore space (or of the pore contours in 2D) from microscopy. This, and the fractal models of permeability were discussed in great detail in my book and related papers [13–15].

2 Basic Concepts

2.1 The Role of Thresholding

The success of any porosity or permeability estimation from a microscopic rock image depends on the reliability of the selected *thresholding algorithm*, the output of which is a binary image whose state 0 (zero bit) will indicate the so-called foreground objects (pores), while state 1 (bit 1) will denote the "background" material (in case of rocks grains and cement). There is no need to describe here the different algorithms in any depth, because the excellent review of thresholding by Sezgin and Sankur [16] is readily available. They discuss and compare more than 40 of the most popular techniques and rank them with respect to their merits, based on several criteria, such as error of misclassification, edge mismatch, nonuniformity, relative foreground area error, shape distortion, etc. In geological applications, one of the most popular thresholding method is still Otsu's [17] clustering algorithm, applied to the gray-value histogram, or one of its more recent modifications [18] for dual- or triple-porosity rocks. Otsu's algorithm is included in the FIJI biological image processing software [19].

If the possible grey values of the pixels are $g = 0, 1, \ldots, \mathrm{G}_{\max}$ ($\mathrm{G}_{\max}$ is generally 255), N is the total number of pixels in the image, denote by $N(i)$ the number of pixels with grey value i. Then $p(i) = \frac{N(i)}{N}$ is the relative frequency of grey values and $P(g)$, their cumulative probability function, is $P(g) = \sum_{i=0}^{g} p(i)$. If T is a *threshold*, one can define the probabilities of the *foreground* and *background* areas as $P_f(T) = \sum_{i=1}^{T} p(i)$; $P_b(T) = \sum_{i=T+1}^{G_{\max}} p(i)$, as well as the average of the pixel values in the foreground or background and their scatter, for example $m_f(T) = \sum_{i=1}^{T} ip(i)$ and $\sigma_f^2(T) = \sum_{i=1}^{T} \left[i - m_f(T)\right]^2 p(i)$. Otsu [17] used a typical "clustering philosophy" in selecting the threshold by maximizing the scatter between background and foreground:

$$T_{\mathrm{opt}} = \arg\max \left\{ \frac{P(T)[1 - P(T)]\left[m_f(T) - m_b(T)\right]^2}{P(T)\sigma_f^2(T) + [1 - P(T)]\sigma_b^2(T)} \right\} \tag{1}$$

For dual-porosity carbonates, the algorithm should be slightly modified, as a third domain must be included for *microporosity* [18,20]. Figure 1 shows results of [20] on two carbonate samples.

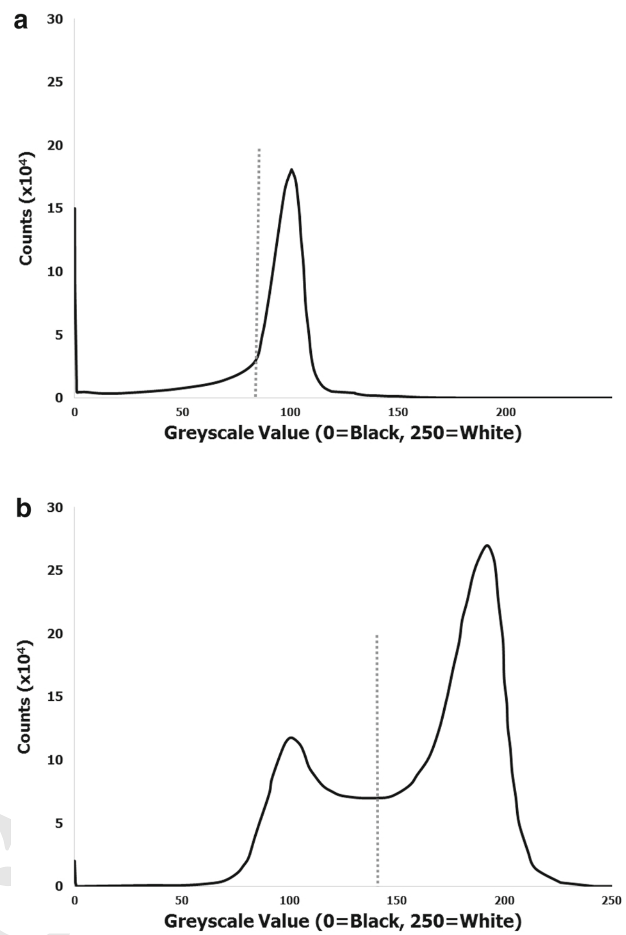

Fig. 1 **a** Gray scale histogram of Indiana limestone (from Bedford, Indiana, USA, 19 % laboratory porosity). *Dotted line* is the threshold which resulted in (13 ± 1) % image porosity (from [20]). **b** Gray scale histogram of pink dolomite (from Edward Plateau, Texas, 29 % laboratory porosity). *Dotted line* is the threshold which resulted in (30 ± 2) % image porosity (from [20])

There are some recent developments since the Review [16], such as [21] where a sliding window entropy filtering is used for nonlinear pore boundary enhancement following binary thresholding.

2.2 Pore Shape Analysis Using Moments

The moments of order (p, q) for any object A having the gray value function $g(x, y)$ is given by

$$m_{p,q} = \iint_A x^p y^q g(x, y)\mathrm{d}x\mathrm{d}y \tag{2}$$

where the integral is over the area of the object [22]. For a binary image (after thresholding) one has

Journal: 13369 MS: 2138 TYPESET DISK LE CP Disp.:2016/4/13 Pages: 21 Layout: Large

$$g(x, y) = F(x, y) = \begin{cases} 1 & \text{if } (x, y) \in \Pi \\ 0 & \text{if } (x, y) \notin \Pi \end{cases} \tag{3}$$

(where Π is the "foreground," i.e., the total set of pores in the microscopic image of the rock) that is the moments are defined as

$$m_{p,q} = \iint_A x^p y^q F(x, y) \mathrm{d}x \mathrm{d}y \tag{4}$$

Special cases of Eq. (4) are [23,24]:

area of the object:

$$A = m_{0,0} = \iint_A F(x, y) \mathrm{d}x \mathrm{d}y \tag{5}$$

center of gravity (x_c, y_c) of the object:

$$x_c = \frac{m_{1,0}}{m_{0,0}}; \quad y_c = \frac{x_{0,1}}{x_{0,0}} \tag{6}$$

If the object is closely elliptical in shape (see Fig. 2), the second-order moments

$$m_{2,0} = \iint_A x^2 F(x, y) \mathrm{d}x \mathrm{d}y;$$

$$m_{0,2} = \iint_A y^2 F(x, y) \mathrm{d}x \mathrm{d}y;$$

$$m_{1,1} = \iint_A xy F(x, y) \mathrm{d}x \mathrm{d}y$$

are also needed to characterize the size, shape, and direction of the best-fitting ellipse, as follows:

semimajor axis of the ellipse:

$$a = \left(\frac{m_{2,0} + m_{0,2} + \left[\left(m_{2,0} - m_{0,2} \right)^2 + 4m_{1,1} \right]^{1/2}}{0.5 m_{0,0}} \right)^{1/2} \tag{8}$$

semiminor axis of the ellipse:

$$b = \left(\frac{m_{2,0} + m_{0,2} - \left[\left(m_{2,0} - m_{0,2} \right)^2 + 4m_{1,1} \right]^{1/2}}{0.5 m_{0,0}} \right)^{1/2} \tag{9}$$

tilt angle of the ellipse:

$$\Phi = \frac{1}{2} \tan^{-1} \left(\frac{2m_{1,1}}{m_{2,0} - m_{0,2}} \right), \tag{10}$$

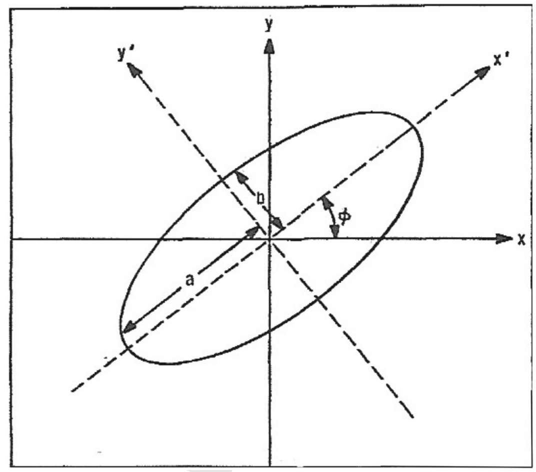

Fig. 2 Parameters of the ellipse defined by a set of pixels (from [23])

where Φ is the angle between the x axis and the semimajor axis, and the principal value of the $\tan^{-1}$ function is selected in a way to insure $-\frac{\pi}{2} \leq \tan^{-1} x \leq \frac{\pi}{2}$.

eccentricity of the ellipse:

$$\varepsilon = \frac{\sqrt{a^2 - b^2}}{a} = \frac{\left(m_{2,0} - m_{0,2} \right)^2 - 4m_{1,1}^2}{\left(m_{2,0} + m_{0,2} \right)^2} \tag{11}$$

Obviously, $0 < \varepsilon < 1$, it is zero for a round object, ~ 1 for an elongated object. The eccentricity ε or aspect ratio b/a can be used to distinguish between different pore types in triple-porosity (e.g., carbonate) rocks.

2.3 Poisson-Distributed Pores

Consider an optical image of total area A_{im} (in mm^2) representing a section of a porous rock, assume that the pores are of random area $A_1, A_2, A_3, \ldots$, and they are two-dimensionally Poisson-distributed with density λ. We shall call λ the *pore density* (in $1/\mathrm{mm}^2$ units), and it is the expected number of pores in a unit area. Denote by Φ the porosity of the image, let $\langle A \rangle$ denote the average ("expected") area of single pore. Then we have the following simple relation between expected porosity $\langle \Phi \rangle$, pore density λ ($1/\mathrm{mm}^2$) and average pore area $\langle A \rangle$ (mm^2):

$$\langle \Phi \rangle \approx \lambda \langle A \rangle \tag{12}$$

Proof Because of the Poisson distribution, the probability that the image area A_{im} contains *exactly N pores* is

$$p_N = \mathrm{e}^{-\lambda A_{\mathrm{im}}} \frac{(\lambda A_{\mathrm{im}})^N}{N!}, \quad N = 0, 1, 2, \ldots \tag{13}$$

Journal: 13369 MS: 2138 TYPESET DISK LE CP Disp.:2016/4/13 Pages: 21 Layout: Large

By Eq. (13) the expected number of pores in the total image is

$$\langle N \rangle == \lambda A_{\mathrm{im}} \tag{14}$$

On the other hand, on any single image porosity is defined as pore area divided by total area (for a planar or 2D rock surface). In a typical case, when the number of pores is close to the expected value $N \approx \lambda A_{\mathrm{im}}$we have

$$\Phi = \frac{\sum_{i=1}^{N} A_i}{A_{\mathrm{im}}} \approx \frac{\sum_{i=1}^{\lambda A_{\mathrm{im}}} A_i}{A_{\mathrm{im}}} = \lambda \frac{\sum_{i=1}^{\lambda A_{\mathrm{im}}} A_N}{\lambda A_{\mathrm{im}}}, \tag{15}$$

which, taking expectations on both sides, proves Eq. (12). (We note that the definition of porosity as $\Phi = \frac{\sum_{i=1}^{\lambda A_{\mathrm{im}}} A_i}{A_{\mathrm{im}}}$ only holds if the pores are non-overlapping).

Equation (12), that is $\langle \Phi \rangle = \lambda \langle A \rangle$ gives an independent way to express permeability in any empirical permeability versus porosity relation in terms of pore density and average pore area. For example, in the celebrated *flow zone index* (*FZI*) equation [25,26]:

$$k = 1014\,(\mathrm{FZI})^2 \left(\frac{\Phi^3}{(1-\Phi)^2} \right), \tag{16}$$

where k is in md; FZI in µm; Φ fraction, one can use $\lambda \langle A \rangle$ as proxy instead of expected porosity $\langle \Phi \rangle$. This might come useful if we do not have an image-analyzing software and only visually observe a large number of pores on the micrograph. If we can *visually* determine the *smallest value* $a = A_{\min}$, the *most frequent value* (*mode*) $b = A_{\mathrm{mode}}$, and the *largest value* $c = A_{\max}$ of the pore areas at a glance, and want a quick-look estimate of the *mean pore area* and its variance without much computation, we can assume that pore areas follow a *triangular distribution* with probability density function

$$f(A; a, b, c, d) = \left(\frac{2}{c-a} \right) \begin{cases} 0 & \text{if } A < a \\ \frac{x-a}{b-a} & \text{if } a \le A < b \\ \frac{c-x}{c-b} & \text{if } b \le A < c \\ 0 & \text{if } c \le A \end{cases},$$

and with known mean value and variance (see [80] p. 80):

$$\begin{aligned} E(X) &= \tfrac{a+b+c}{3} \\ \mathrm{Var}(X) &= \tfrac{a^2+b^2+c^2-ab-ac-bc}{18} \end{aligned}$$

3 Kozeny–Carman Equations

3.1 Concepts of Specific Surface Area

By the Kozeny–Carman ("KC") equation, (Carman, [1]) the permeability of a porous sedimentary rock is given by

$$k = \frac{1}{b} \Phi^3 \frac{1}{S_{\mathrm{spec}}^2} \frac{1}{\tau^2} \tag{17}$$

where b is a shape factor of order one, $\Phi \in [0, 1]$ is porosity, S_{spec} is specific surface area defined as total surface area per unit bulk volume, τ is tortuosity. Combining $\frac{1}{b\tau^2}$ to a single constant C, the KC law is expressed as

$$k = C \frac{\Phi^3}{S_{\mathrm{spec}}^2} \tag{18}$$

In sedimentology, there are three different concepts of specific surface area [2,3], namely

S_{spec} = surface area per unit bulk volume of the rock; S_0 = surface area per unit volume of solid material; S_p = surface area per unit volume of pore space.

The three measures of specific surface area are interrelated. For an arrangement of spherical grains of the same radius r we have:

Theorem 1 *For any arrangement of porosity Φ consisting of spherical grains of the same radius r one has*

$$S_{\mathrm{spec}} = (1-\Phi) S_0; \quad S_{\mathrm{spec}} = \Phi S_p; \quad S_p = \frac{1-\Phi}{\Phi} S_0 \tag{19}$$

Proof Take a unit bulk volume of the rock, $(1-\Phi)$ part of it consists of solid material which contains $n = (1-\Phi) : \frac{4r^3\pi}{3}$ grains, that is the total surface in unit bulk volume is

$$S_{\mathrm{spec}} = n \cdot 4r^2\pi = \frac{3(1-\Phi)}{r} \tag{20}$$

A unit grain volume contains $N = 1 : \frac{4r^3\pi}{3}$ grains, which have a total surface area

$$S_0 = N \cdot 4r^2\pi = \frac{3}{r}, \tag{21}$$

and from Eqs. (20, 21) one has $S_{\mathrm{spec}} = (1-\Phi)S_0$ as stated. Now, take a bulk volume V_b of rock in such a way that its pore space occupies a unit total volume, that is $V_b \Phi = 1$, whence $V_b = \frac{1}{\Phi}$. The total surface associated with this unit pore volume is $S_p = V_b S_{\mathrm{spec}} = \frac{S_{\mathrm{spec}}}{\Phi}$, that is $S_{\mathrm{spec}} = \Phi S_p$ as stated. The third equation in Eq. (19) follows from the first two.

Journal: 13369 MS: 2138 ☐ TYPESET ☐ DISK ☐ LE ☐ CP Disp.:2016/4/13 Pages: 21 Layout: Large

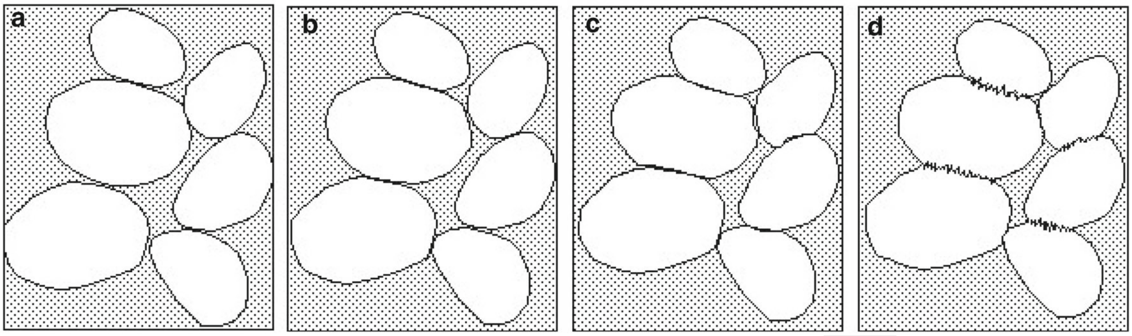

Fig. 3 Tangential (**a**), flattened (**b**), concavo-convex (**c**) and sutured (**d**) intergranular (sutured) contacts as seen in thin section (from [27])

Note The simple relations (Eq. 19) between the three kinds of specific surface areas are only true for *tangential* contacts between the grains, as shown in Fig. 3.

In terms of the different concepts of specific surface area, the KC equation can be put in three forms (which are equivalent only for grains of equal size in tangential contact):

$$k = C\frac{\Phi^3}{S_{\text{spec}}^2} \tag{22a}$$

$$k = C\frac{\Phi^3}{(1-\Phi)^2\, S_0^2} \tag{22b}$$

$$k = C\frac{\Phi}{S_p^2} \tag{22c}$$

where $C = \frac{1}{b\tau^2}$. The estimation of τ (tortuosity) from digital rock images will be discussed in Sect. 3.3.

3.2 The Use of BET Surface Areas in the Kozeny–Carman Equation

If we want to estimate permeability by using BET-derived specific surface areas in the KC equation (as in [28,29]), we write the KC equation in the form

$$k = C \cdot \frac{\Phi^3}{\left(1-\Phi^2\right) S_s^2} \tag{23}$$

where S_s is grain-related specific surface area, defined as surface area per unit grain volume. S_s (in μm^{-1} units) is computed from the measured BET specific grain surface S_g (in m^2/g units) as

$$S_s = S_g \rho_g \tag{24}$$

In Eq. (23) the factor C is the *Kozeny factor* (which depends on tortuosity and on the cross-sectional shape of the tubes). It can be estimated from porosity via a simple model [28] of a linear 3D system of interpenetrating circular tubes, as

Table 1 Kozeny factor C by Eq. (25) from [28]

Φ%	c
0	0.17
20	0.21
40	0.24
60	0.27
80	0.33
100	0.50

$$C = \left[4\cos\left\{\frac{1}{3}\arccos\left(\Phi\cdot\frac{64}{\pi^2}-1\right)+\frac{4}{3}\pi\right\}+4\right]^{-1} \tag{25}$$

(see Table 1, from [28]) (Table 1).

3.3 Tortuosity Estimation for the KC Equation

3.3.1 Scaling of Tortuosity

We first show with a simple scaling argument that the hydraulic tortuosity in 2D sections of granular porous sedimentary rocks is an increasing function of sample size. Let L be the vertical size of the section considered (assuming that hydraulic flow goes from top to bottom); Φ porosity (in fraction); τ tortuosity (defined as the expected ratio of hydraulic path length to Euclidean length between 2 randomly selected points, always $\tau \geq 1$); r_0, P_0, A_0 characteristic *size*, characteristic *perimeter*, characteristic *area* of the grains (in the 2D section); Z average number of pores adjacent to a grain (in the 2D section). We shall denote by $D_{P/A}$ the exponent in the celebrated Mandelbrot's *perimeter-area scaling law* [13,30,31] applied to the ensemble of the grains in the microscopic 2D section:

$$P = P_0\left(\frac{\sqrt{A}}{r_0}\right)^{D_{P/A}} \tag{26}$$

Theorem 2 *The average hydraulic path of a flow from top to bottom is given by the equation*

$$\left\langle \frac{L_{\text{hydr}}}{L} \right\rangle = \tau = \Phi + \frac{(1-\Phi)}{Z}\left(\frac{P_0}{r_0}\right)\left(\frac{\sqrt{A}}{r_o}\right)^{D_{P/A}} \tag{27}$$

Note that for $\Phi = 1$ we have $\tau = 1$; for $\Phi = 0$ there are no pores at all, that is $Z = 0$ and consequently $\tau = \infty$ as it should be. (*The divergence of tortuosity in low-porosity, low permeability clay-bearing sandstone was noted in* [13,14].)

Equation (27) is proven by a heuristic scaling argument. Along a randomly selected top-to-bottom vertical line of length L by the *De-Lesse principle* [32] a total length ΦL of the line would go through pore space. Across these parts of the line, the flow goes along straight line segments. The remaining $(1-\Phi)\,L$ length of the vertical line is filled by grains, the fluid path would cross $\frac{(1-\Phi)L}{r_0}$ grains if it could flow along a straight vertical line. But it cannot proceed straight, but every time the flow reaches a grain it changes direction and continues in a "throat" following the curvature of the grain's perimeter. By the definition of *the grain/pore coordination number Z*, the periphery P of a grain is adjacent to Z other grains, so that every individual "detour" adds a length $\left(\frac{P}{Z}\right)$ to the hydraulic path. This *detour* is, by Mandelbrot's Eq. (26) equal to $\left(\frac{P}{Z}\right) = \frac{P_0}{Z}\left(\frac{\sqrt{A}}{r_0}\right)^{D_{P/A}}$. As there are $\frac{(1-\Phi)L}{r_0}$ such *detour*s, the total hydraulic length from top to bottom is $L_{\text{hydr}} = \Phi L + \frac{(1-\Phi)L}{Z}\left(\frac{P_0}{r_0}\right)\left(\frac{\sqrt{A}}{r_0}\right)^{D_{P/A}}$, what is the same as Eq. (27) to be proved.

As Eq. (27) is a new result, it should be compared with other theoretical models of tortuosity, where there is explicit or implicit dependence on porosity. In the Lattice Gas (LG) model of Koponen et al. [33], $\tau = 0.8(1-\Phi) + 1$; in the percolation model [34] of the same group $\tau = 1 + a\frac{(1-\Phi)}{(\Phi-\Phi_c)^m}$ (a and m are fitting parameters). Comiti and Renaud [35] assumed cube-shaped grains and obtained $\tau = 1 + P\ln\left(\frac{1}{\Phi}\right)$ (P a fitting parameter). Yu's [36] well-cited 2D model is based on square-shaped grains and yields the scaling law $\tau = \left(\frac{L}{\lambda_{\min}}\right)^{D_T - 1}$ where the tortuosity dimension is $D_T = 1 + \frac{\ln \tau_{av}}{\ln \frac{L}{\lambda_{av}}}$ [the porosity dependence enters through the term "τ_{av}" which is a complicated function of porosity ([36], Eq. (2))].

3.3.2 Estimation of Hydraulic Tortuosity from Binarized Rock Image

The pores in a 2D micrograph almost never form a connected percolating path from one side to opposite side of the image, even in good-permeability reservoir sandstones such as the one shown in Fig. 4.

This is due to the fact that the pore space is embedded in the 3D Euclidean space and a percolating path would "jump out" several times from the image's plane if there is an obstacle

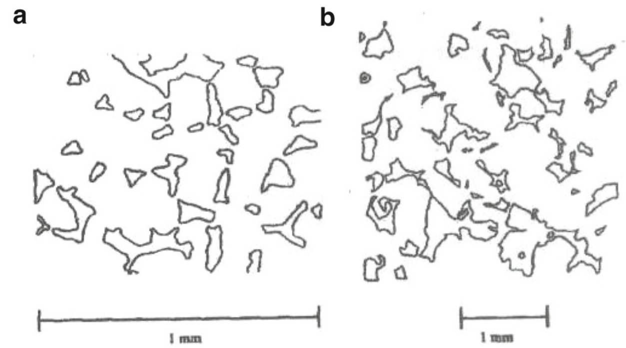

Fig. 4 2D pore contours, from [37]. **a** Berea sandstone reproduced from [38]; **b** Massilon sandstone from [39]

(a grain), continue its path in pore space below or above the grain, then return again to the original plane where its endpoints P and Q are. As we are working with a 2D image, the best we can do is to estimate the length of the projection of the real 3D path onto the 2D plane where the endpoints of the path are, or *move the pores on the image plane without rotation until they touch and form a continuous path*. We assume that for reservoir rocks this will give a reasonable estimate for tortuosity.

3.3.2.1. Use of the Method of Moments

Some image processing programs such as Kilian's [40] software (based on Teague's, [23], *method of moments* discussed in Sect. 2.2) can compute for every pore (of number i) the length l_i of its major axis and estimate the angle ϑ_i, $(-90° \leq \vartheta_i \leq 90°)$ what this axis makes with the horizontal reference direction X. (See Fig. 2; Eqs. 8, 10).

Take two points, P, Q randomly and far from each other in the rectangle $XY = \{(x.y)|0 \leq x \leq X_{\max}; 0 \leq y \leq Y_{\max}\}$. Consider the 2D projection of a typical hydraulic path from P to Q consisting of line segments. In most cases, the projected line segment would coincide with the longer axis $l_i = 2a_i$ of some pore in the XY plane. The broken line consisting of the segments l_i is the "skeleton" of a chain of touching pores, which are either in the XY plane or immediately below or above it in a thin slab S of thickness Δ: $S = \left\{(x, y, z)|(x, y) \in XY; -\frac{\Delta}{2} \leq z \leq \frac{\Delta}{2}\right\}$. Because of the local homogeneity of the rock sample, we assume that (i) the probability distributions of the major axis lengths $\{l_i\}$ and of their directions $\{\vartheta_i\}$ are the same on the XY rectangle as in the slab S. We also assume that (ii) $\{l_i\}$ and $\{\vartheta_i\}$ are both independent random variables and $\{l_i\}$,$\{\vartheta_i\}$ are also independent of each other and that (iii) $\langle\vartheta_i\rangle = 0$, $\langle\sin\vartheta_i\rangle = 0$ (where angular brackets mean expected value), as well as that (iv) for $i \neq j$ we have $\langle\cos\vartheta_i \cos\vartheta_j\rangle = \langle\cos\vartheta\rangle^2$. "Expected value," in this context means expected value over all statistically equivalent possible random realizations of the microscopic image.

We define a random tortuosity τ as follows. Let $n = 1$, and construct a *random chain of n pores* starting from a fixed point P. We select pores randomly from among the actual pores figuring on the *XY* section, move them without rotation and any change in their shape into positions where they touch each other and form a continuous hydraulic path from P to some random endpoint what we call Q. A particular pore in the chain has a major axis of length l_i and of direction angle ϑ_i, that is the X- resp. Y-projections of the major axis are $\xi_i = l_i \cos\vartheta_i$, $\eta_i = l_i \sin\vartheta_i$, $i = 1, 2, \ldots, n$. The tortuosity of this particular hydraulic path is

$$\tau = \frac{\sum_{i=1}^{n} l_i}{\sqrt{\left(\sum l_i \cos\vartheta_i\right)^2 + \left(\sum l_i \sin\vartheta_i\right)^2}}. \tag{28}$$

If n is large, and we assume ergodicity, the expected (average) tortuosity over all possible chains consisting of n pores is the same as the expectation over all realizations. We get:

$$\langle\tau\rangle = \left\langle \frac{\sum_{i=1}^{n} l_i}{\sqrt{\left(\sum l_i \cos\vartheta_i\right)^2 + \left(\sum l_i \sin\vartheta_i\right)^2}} \right\rangle \tag{29}$$

If for all pores on the image the length of their major axis l and its direction ϑ are known, Eqs. (28, 29) can be used to compute tortuosity by Monte Carlo (as it will be suggested in 3.3.2.3). A very simple and efficient approximate estimation of $\langle\tau\rangle$ can be given as follows, using the notation $l = \langle l_i\rangle$and making use of the assumptions (i) to (iv). Because of assumption (ii) the variables $\{l_i\}$ and $\{\vartheta_i\}$ are independent, and the expected value of the fraction is well approximated by its expected numerator divided by the expected denominator:

$$\begin{aligned}
\langle\tau\rangle &= \left\langle \frac{\sum_{i=1}^{n} l_i}{\sqrt{\left(\sum l_i \cos\vartheta_i\right)^2 + \left(\sum l_i \sin\vartheta_i\right)^2}} \right\rangle \\
&\approx \frac{\left\langle\sum_{i=1}^{n} l_i\right\rangle}{\sqrt{\left\langle\left(\sum l_i \cos\vartheta_i\right)^2 + \left(\sum l_i \sin\vartheta_i\right)^2\right\rangle}} \\
&\approx \frac{nl}{\sqrt{\sum_i \left(\cos\vartheta_i^2 + \sin\vartheta_i^2\right) + \sum_{i\neq j}\left\langle\cos\vartheta_i \cos\vartheta_j\right\rangle + \sum_{i\neq j}\left\langle\sin\vartheta_i \sin\vartheta_j\right\rangle}} \\
&\approx \frac{nl}{l\sqrt{n + n(n-1)\left\langle\cos\vartheta\right\rangle^2}} \\
&\approx \frac{1}{\langle\cos\vartheta\rangle}
\end{aligned} \tag{30}$$

where we used assumptions (ii), (iii) and (iv) and took the limit $n \to \infty$. The approximate rule what we obtained (valid for $n = 1$), that is

$$\langle\tau\rangle \approx \frac{1}{\langle\cos\vartheta\rangle}, \tag{31}$$

can be expressed in words as: *the average tortuosity is the reciprocal of the average direction cosine of the major axes of the pores on the 2D microscopic image*.

3.3.2.2. Numerical Check of Eq. (31)

As a numerical check, I measured the major-axis lengths and their directions (with respect to the X axis) of the thirty-three (33) pores in a Berea sandstone micrograph shown in Fig. 4 (from [38]).

Figure 5 shows the 33 pores, their major-axis lengths l_i, and direction angles ϑ_i. The results are compiled in Table 2. Note that the l_i and $\sin\vartheta_i$ values are not needed for the computation of $\langle\cos\vartheta\rangle$, I only listed them as they will be used in the Monte Carlo estimation of $\langle\tau\rangle$ based on Eq. (28). The obtained average tortuosity $\langle\tau\rangle \approx \frac{1}{\langle\cos\vartheta\rangle} = 1.6$ is close to the median value of tortuosity reported in [41] for Berea sandstone (see Table 3).

In words. Eq. (31) tells that we should take *all* the N pores in the image, compute their direction (that is the angle ϑ between their major axis and the X-axis), compute the average of the direction cosines $\langle\cos\vartheta\rangle = \frac{1}{N}\sum_{k=1}^{N}\cos\vartheta_i$and then the average tortuosity will be given by $\langle\tau\rangle \approx \frac{1}{\langle\cos\vartheta\rangle}$. Equation (31) correctly expresses that always $\langle\tau\rangle \geq 1$, and it also predicts that tortuosity can be different in the 3 mutually perpendicular directions X, Y, Z, which is in accordance with recent experimental findings (see Table 3 reproduced from [41]) on anisotropic permeability, and is along the lines of the TCT (*tensorial connectivity-tortuosity*) concept of Zhang et al. [42]. In this case, of course, permeability, which is expressed by the Kozeny–Carman equation ([43], p. 104) as

$$k = \frac{1}{b}\Phi^3 \frac{1}{S_{\text{spec}}^2}\frac{1}{\tau^2} \tag{32}$$

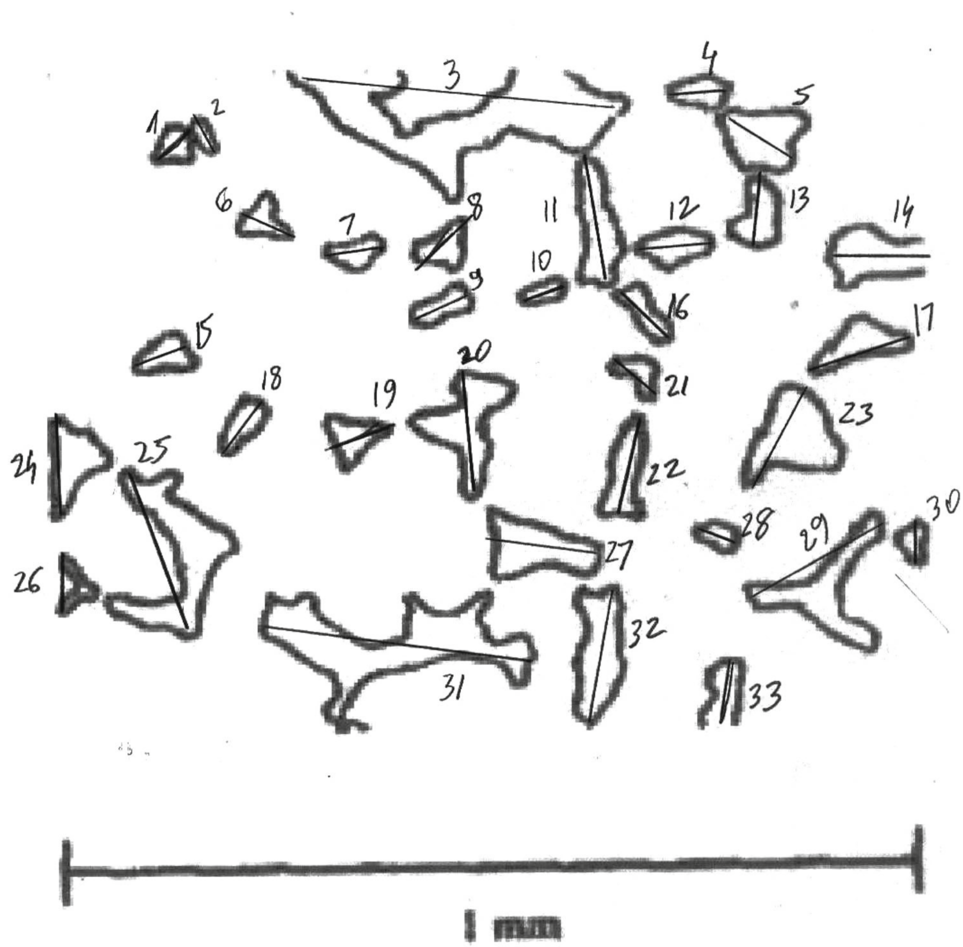

Fig. 5 Berea sandstone micrograph, major-axis lengths and directions (the micrograph is from [38])

becomes a direction-dependent tensorial quantity, because the presence of the $\langle \cos \vartheta \rangle$ factor in the tortuosity equation (31) makes it dependent on the direction of the X axis.

3.3.2.3. Monte Carlo Calculation of Tortuosity

The algorithm for the Monte Carlo calculation of tortuosity using Eqs. (28, 29) is straightforward. Suppose we consider hydraulic paths traversing n pores, where $n \gg 1$ might be larger than the number of pores in the image. Denote by N the number of pores in the image, let $M \gg 1$ be a large integer. Select n pores randomly out of the altogether N pores of the image, with possible repetitions, for example by calling n times a random number generator (RND) routine that each time returns a different uniform random value $0 \leq x < 1$. Divide the unit interval to N disjoint parts of equal length

$$P_i = \left[\frac{i-1}{N}, \frac{i}{N}\right), \quad i = 1, 2, \ldots, N; \quad \bigcup_{i=1}^{N} P_i = [0, 1) \tag{33}$$

If the randomly generated x value lies in the subinterval P_i, then in the sum (Eq. 28) we select the ith values of l_i, $\cos \vartheta_i$, $\sin \vartheta_i$. After this, for the given experiment tortuosity is computed by Eq. (28) as $\tau = \frac{\sum_{i=1}^{n} l_i}{\sqrt{\left(\sum l_i \cos \vartheta_i\right)^2 + \left(\sum l_i \sin \vartheta_i\right)^2}}$. To get the expected value of tortuosity, we repeat this experiment $M \gg 1$ times, and define $\langle \tau \rangle$as the average, $\langle \tau \rangle = \frac{1}{M} \sum_{k=1}^{M} \tau_k$ where τ_k is the tortuosity in the kth random experiment. If necessary, the SD (standard deviation) and other statistics of τ can also be computed.

As an example for the MC computation of Eq. (28) for the Berea sandstone (Fig. 5; Table 2), I selected $n = 10$, and the data for $N = 33$ pores. In the first experiment, the random number generator returned pore numbers 20, 28, 2, 21, 30, 4, 31, 25, 31,16 (note that #31 occurs twice) and Eq. (28) yields $\tau = \frac{\sum_{i=1}^{n} l_i}{\sqrt{\left(\sum l_i \cos \vartheta_i\right)^2 + \left(\sum l_i \sin \vartheta_i\right)^2}} = \frac{1339}{651.1306} = 2.056$ (a reasonable value!). Repeating this, say $M = 20$ or 30 times, and taking the average, a good approximation of $\langle \tau \rangle = \frac{1}{M} \sum_{k=1}^{M} \tau_k$ would be obtained.

4 Timur's Equation and Timur-Type Equations

In a classic paper, Chevron Petrophysicist Aytekin ("Turk") Timur [2,3] attempted to express the permeability of 155

Table 2 Determination of the average tortuosity for Berea sandstone from Fig. 5, using Eq. 31

#	l_i micron	ϑ_i (°), angle from horizontal axis	$\cos\vartheta_i$	$\sin\vartheta_i$
1	50	41	0.75	0.71
2	50	−62	0.47	−0.88
3	388	−5	0.996	−0.09
4	75	5	0.996	0.09
5	94	−30	0.87	−0.5
6	63	−27	0.89	−0.045
7	69	16	0.96	0.28
8	75	50	0.64	0.77
9	69	30	0.87	0.5
10	50	21	0.93	0.36
11	144	−80	0.17	−0.98
12	81	5	0.996	0.09
13	75	87	0.05	0.999
14	119	2	0.999	0.03
15	56	20	0.94	0.34
16	75	−50	0.64	−0.77
17	125	20	0.94	0.34
18	75	51	0.63	0.78
19	69	18	0.95	0.30
20	144	−85	0.087	−0.996
21	63	−40	0.77	0.64
22	119	78	0.21	0.978
23	125	61	0.48	0.875
24	119	88	0.03	0.999
25	200	72	0.31	0.95
26	75	90	0	1
27	131	−8	0.99	−0.14
28	50	−25	0.91	−0.42
29	175	30	0.87	0.5
30	44	−90	0	−1
31	319	−8	0.99	−0.14
32	156	80	0.17	0.98
33	69	80	0.17	0.98
Ave	$\langle l_i\rangle = 107\mu$	$\langle\vartheta\rangle = 8.8^o$	$\langle\cos\vartheta\rangle =$ 0.62648 Tortuosity estimate by Eq. 31: $\langle\tau\rangle \approx \frac{1}{\langle\cos\vartheta\rangle} = 1.6$	

sandstone samples from 3 oilfields in North America in the empirical form $k = ax^b$ where "x" was an expression dependent on *both* porosity Φ and *irreducible water saturation* S_{wi}. For "x" he selected the following five different expressions figuring in the routine permeability equations current in those days:

Table 3 Experimentally found tortuosities in 3 main directions, for Berea sandstone, at atmospheric pressure (from [41])

Direction	$\tau_{\min}$	τ_{median}	$\tau_{\max}$
X	1.5	1.795	2.34
Y	1.54	1.79	2.46
Z	1.49	1.74	2.40

(a)

$$x = \frac{\Phi^6}{S_{wi}^2}. \tag{34a}$$

(This term comes from an equation $k = 6.25 \times 10^{-4}\frac{\Phi^6}{S_{wi}^2}$ used by Sclumberger Co., [44])

(b)

$$x = \frac{\Phi^3}{S_{wi}^2} \tag{34b}$$

(Same as the KC Eq. 22, but $S_{\text{spec}}$is substituted by S_{wi})

(c)

$$x = \frac{\Phi^3}{(1-\Phi)^2\, S_{wi}^2} \tag{34c}$$

(Same as the KC Eq. 22, but S_0 is substituted by S_{wi})

(d)

$$x = \frac{\Phi}{S_{wi}^2} \tag{34d}$$

(Same as the KC Eq. 22, but $S_p$is substituted by S_{wi})

(e)

$$x = \frac{\Phi^{4.4}}{S_{wi}^2} \tag{34e}$$

(An equation found by Timur from an assumed general relation $k = \alpha\frac{\Phi^\beta}{S_{wi}^\gamma}$, by optimizing the α, β, γ fitting parameters.)

Timur [2,3] obtained the best fit with measured data using Eq. (34e), and today (see e.g., the compilation of permeability equations in [45]) the following formula is called "Timur equation" in Petroleum Industry

$$k = 0.136\frac{\Phi^{4.4}}{S_{wi}^2} \tag{35}$$

(k in mD, Φ in %, S_{wi} in %).

Journal: 13369 MS: 2138 TYPESET DISK LE CP Disp.:2016/4/13 Pages: 21 Layout: Large

There have been many other attempts to express permeability in terms of *irreducible water saturation* S_{wi}, the most famous equations are (from [45]):

$$k = \left(100 \frac{\Phi^{2.25}}{S_{wi}}\right)^2, \tag{36}$$

(k in mD, Φ in fraction, S_{wi} in fraction—the so-called Wyllie and Rose 1st equation [46]);

$$k = \left(100 \frac{\Phi^2 (1 - S_{wi})}{S_{wi}}\right)^2, \tag{37}$$

(k in mD, Φ in fraction, S_{wi} in fraction—the so-called Wyllie and Rose 2nd equation [46]);

$$x = \frac{C\Phi^3}{S_{wi}^2}, \tag{38}$$

(k in mD, Φ in fraction, S_{wi} in fraction, C is a constant, for oil $C = 250$, for gas $C = 80$—this is the so-called Morris and Biggs equation [47]).

Some further Timur-type equations (from [48]) are:

$$k = 62.5 \frac{\Phi^6}{S_{wi}^2}, \quad \text{Tixier equation [49]} \tag{39}$$

$$k = 4.90 \frac{\Phi^4 (1 - S_{wi})^2}{S_{wi}^4}, \text{ Coates Equation [50].} \tag{40}$$

The main difference between Timur-type and KC equations is that in the Timur-type equations *irreducible water saturation* S_{wi} (what is strictly speaking a *non-geometric quantity*) is used instead of *specific surface area*. By Darcy's Law, the physical dimension of permeability is length-squared ([m^2]), but this correct dimension only appears in the KC equation, because all three kinds of specific surface areas $S_{\text{spec}}, S_0, S_p$ have the dimension area/volume $= [1/m]$ in Eqs. (19). In the Timur-type equations S_{wi} is dimensionless, leading to a dimensionless permeability. Leaving this question apart (assuming that the constant factor in the Timur-type equations takes care of the missing dimensions), we turn to the main topic of the *Review*, and discuss how to predict *irreducible water saturation* from the microscopic rock image.

4.1 Monte Carlo Prediction of S_{wi} from Microscopic Rock Images

There is a general consensus [48] that irreducible water is distributed on the *wetted areas* of the grain surface (directly on the grain surface, or inside the grain-lining clay layer), that is we can assume that $S_{wi} = cS_p$ where S_p is surface area *per unit volume of pore space*, and c is a constant. This assumption excludes such parts of the grain surface (seen in Fig. 3b–d) which have no direct contact with water and thus cannot contribute either to permeability, or to the irreducible water content.

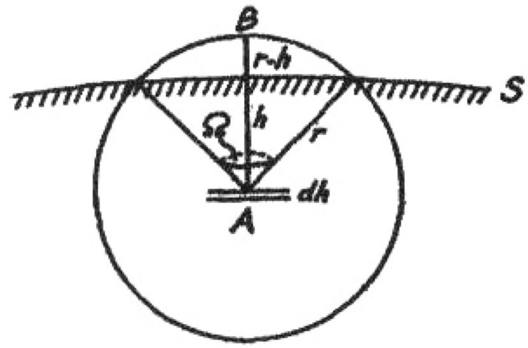

Fig. 6 Illustrating the proof of Eq. (41) (after [51])

We propose a new, *Monte Carlo algorithm* to find S_{wi}, based on the following theorem.

Theorem 3 *Select in the image of an isotropic porous rock two randomly placed points A and B a distance r apart, where r is small, $r \ll 1$. Then the probability that A and B are in different media* (i.e., one is in a pore, the other in a grain) *is given by*

$$\Pr(A\&B \ \ are \ \ in \ \ different \ \ media) = S_p \frac{r}{2}, \tag{41}$$

where $\Pr(X)$ *is the probability of the event* X. *The proof is purely geometric and follows an idea of Debye et al.* [51], *using the geometry in Fig. 6.*

Consider a finite volume of rock, with total pore surface area $S_{\text{area}}(\Pi)$, total pore volume $V(\Pi)$, where Π is the total pore space. Let Γ be the total space occupied by grains. Suppose A is in Π, B in Γ and $\overline{AB} = r \ll 1$. Let the segment AB move in such a way that it follows the pore surface S while keeping A and B always in different media. Then point A must always be some distance $h < r$ away from the surface S. If the distance of A from S is between h and $h + \mathrm{d}h$, the total pore volume where A can be is $S_{\text{area}}(\Pi)\mathrm{d}h$. For any fixed position of A, the direction of the AB segment must be within a certain solid angle to assure that it crosses S. Using the equation for the surface area of the spherical cap, the probability that the AB radial segment intersects S is $\frac{S_{\text{area}}(\Pi)\mathrm{d}h}{V(\Pi)} \cdot \frac{2\pi r(r-h)}{4\pi r^2} = S_p \cdot \frac{2\pi r(r-h)}{4\pi r^2}$ and the probability that A and B are in different media is

$$\Pr(A\&B \text{ are in different media}) = 2S_p \int_0^r \frac{r-h}{2r}\mathrm{d}h = \frac{S_p r}{2},$$

Table 4 Table 4 (after [56])

Dimension of fracture sets	Size of matrix blocks	l_{fm}	l_{fv}	l_{vm} for the case of Fig. 7
One-dimensional	A	$l_{fm} = A/6$	$l_{fv} = l_x$	$l_{vm} = a/6$
Two-dimensional	A, B	$l_{fm} = \frac{AB}{4(A+B)}$	$l_{fv} = \frac{l_x+l_y}{2}$	$l_{vm} = \frac{ab}{4(a+b)}$
Three-dimensional	A, B, C	$l_{fm} = \frac{3ABC/10}{AB+BC+CA}$	$l_{fv} = \frac{l_x+l_y+l_y}{3}$	$l_{vm} = \frac{3abc/10}{ab+bc+ca}$

All variables are defined in Figs. 7, 8 and 9. In the 5th column a, b, c are spacings between small fractures in the x, y, z directions, respectively

as stated. (The factor "1/2" arises because A and B are interchangeable).

Using Theorem 3, the specific surface S_p can be estimated by *Monte Carlo* (MC) as follows: Suppose the four corners of the rock image are, clockwise, at $(0, Y)$; (X, Y); $(X, 0)$; $(0, 0)$; let $r_{\max}$ be a small positive value. Select a large integer number N (1000 or larger), this will be the number of experiments for a given AB distance $\overline{AB} = r \leq r_{\max}$. If the subroutine RND returns at each subsequent call different and independent random numbers uniformly distributed in [0, 1), the MC algorithm proceeds as follows:

1. Select $r \in [0, r_{\max})$ randomly as
$$r = \text{RND} \cdot r_{\max} \tag{42}$$
2. Define the four corner points $P_1\,(x_1, y_1)\,, \ldots, P_4\,(x_4, y_4)$ which are placed by a distance r inside from the image's boundary (for example: $P_2 = (X - r, Y - r)$.
3. Place the point $A = \left(A_x, A_y\right)$ randomly inside the rectangle $P_1 P_2 P_3 P_4$ as:
$$\begin{aligned} A_x &= x_3 + \text{RND} \cdot (x_4 - x_3) \\ A_y &= y_3 + \text{RND} \cdot (y_1 - y_3) \end{aligned} \tag{43}$$
4. Place the point $B = \left(B_x, B_y\right)$ inside the larger rectangle $(0, Y)$; (X, Y); $(X, 0)$; $(0, 0)$ at a distance r from A in a random direction from it, as:
$$\begin{aligned} B_x &= A_x + r\cos(\text{RND} \cdot 2\pi) \\ B_y &= A_y + r\sin(\text{RND} \cdot 2\pi) \end{aligned} \tag{44}$$
(Note that the point $B = \left(B_x, B_y\right)$ will remain inside the image.)
5. The placement of points A and B, that is the computation of Eqs. (43, 44) should be made with pixel precision.
6. Call the experiment "successful" if A and B do not lie in the same medium, that is if one of them is in grain, the other in pore.
7. Repeat the experiment (from steps 3 to 6) N times for the same value of r and count how many times have you got "success," that is A&B were in different media.
8. Estimate the probability Pr($A\&B$ are in different media) subject to the condition $\overline{AB} = r$ as
$$\text{Pr}\ (A\&B \text{ are different}|\ \overline{AB} = r) = \frac{N_{\text{success}}}{N} \tag{45}$$
9. Repeat this (from Step 1 to 8) with about 10 different small r values. Using the theoretical equation (41) one expects a linear relation
$$\text{Pr}(\,A\&B \text{ are in different media}|\ \overline{AB} = r) = S_p \frac{r}{2} \tag{19}$$
that is, from the *Probability* versus r plot the specific pore surface can be determined from the slope of this line.

4.2 How to Use Timur's Model?

For a review of Timur's equation ([2,3]) see [48] (that also lists further similar equations such as Tixier [49], Wyllie and Rose [46] to estimate permeability from measured irreducible water saturation S_{wi} or vice versa). In Timur's equation permeability k and S_{wi} are connected as $k = \frac{0.136\Phi^{4.4}}{S_{wi}^2}$ (Eq. 35) where k is in md, Φ is in %, S_{wi} is irreducible water saturation in percentage of the pore volume. The main problem in applying this equation to a microscopic rock image is that S_{wi} is not known. Physically, one can express S_{wi} as $S_{wi} = 100 \cdot \frac{P_t \cdot (\text{pix}_{\text{size}}) \cdot \delta}{A_t \cdot (\text{pix}_{\text{size}})^2} = 100 \cdot \frac{P_t \delta}{A_t \text{pix}_{\text{size}}}$ (Eq. 45), where P_t is total perimeter (of all types of void spaces on the image) in pixel-size unit, A_t is total area (of all types of void spaces on the image) in pixel-area unit, pix_{size} is pixel size, δ is thickness of the non-removable water which is adsorbed on the grain surfaces. Of course, δ depends on grain surface roughness, on the wettability of the minerals and on the chemical composition of the water, and can range from the diameter of a single water molecule (2.75 Å $= 0.275$ nm) to a few thousands of nanometers. A recent measured value for the thickness of nanoscale adsorbed brine film on silica surface ([52]) is reported between 249 and 265 nm. Taking the average value $\delta = 257$ nm, and a pixel size $\text{pix}_{\text{size}} = 20\,\mu\text{m} = 20{,}000$ nm, then—for a typ-

Journal: 13369 MS: 2138 ☐ TYPESET ☐ DISK ☐ LE ☐ CP Disp.:2016/4/13 Pages: 21 Layout: Large

ical micrograph—we get $S_{wi} = 100 \cdot \frac{P_t \delta}{A_t \mathrm{pix}_{\mathrm{size}}}$. If the total porosity is Φ, by Timur's Eq. (35): $k = \frac{0.136\Phi^{4.4}}{S_{wi}^2}$.

Of course, we cannot know for sure that in the given rock one really has $\delta = 257\,\mathrm{nm} = 0.257\,\mu\mathrm{m}$, though the order of magnitude of this value seems reasonable because Adams et al. (Table 4 in [53]) reported similar RMS surface roughness for sand grains (0.269 µm) and the thickness of adsorbed water should be *around the same* as the RMS surface roughness (as noted in [52]). A more reasonable permeability is obtained if one assumes that the thickness of adsorbed water is the same as the *peak-to-valley roughness* of the grain contours, which was found experimentally ([53]) $1.89\,\mu\mathrm{m} = 1890\,\mathrm{nm}$ for sand grains. Assuming for δ the value $\delta = 2000\,\mathrm{nm} = 2\,\mu\mathrm{m}$ we get $S_{wi} = 100 \cdot \frac{P_t \delta}{A_t \mathrm{pix}_{\mathrm{size}}}$; and using Timur's Eq. (35): $k = \frac{0.136\Phi^{4.4}}{S_{wi}^2}$.

By SEM microscopy, the actual value of grain surface roughness can be estimated. If no measured δ-value is known, I recommend to apply Timur's method with $\delta = 2000\,\mathrm{nm} = 2\,\mu\mathrm{m}$ as *default*.

Another reasonable approach would be to consider δ as a *fitting parameter*, and determine it from an image where the permeability of the sample k is already known from an independent laboratory measurement, using the equation

$$k = 0.136\Phi^{4.4} \Big/ \left[100 \cdot \frac{P_t}{A_t} \frac{\delta}{\mathrm{pix}_{\mathrm{size}}}\right]^2. \tag{46}$$

Then for other images (of the same lithology) the δ-value obtained from Eq. 46 could be used.

4.3 The Timur Equation Approach, Using BET Surface Areas

Timur's equation can be used to estimate permeability k from measured irreducible water saturation S_{wi}(or *vice versa*, to estimate S_{wi} from k). In Timur's equation permeability k and S_{wi} are connected as $k = \frac{0.136\Phi^{4.4}}{S_{wi}^2}$ (35), where k is in md, Φ is in %, $S_{wi}$is irreducible water saturation in % of the pore volume. The main problem in applying this equation is how to find S_{wi}. We can express S_{wi} (in %) as

$$S_{wi} = 100 \cdot S_p \cdot \delta, \tag{47}$$

where S_p is the *specific surface per unit pore volume*, and δ is thickness of the *non-removable water* adsorbed on the pore walls.

For the application of Eqs. (35) and (47), in addition to the value of δ and Φ, we also need the value of S_p, that is the *specific surface per pore volume*. Suppose that according to the BET (Brunauer–Emmett–Teller, [54]) gas adsorption measurement the specific grain surface is S_g in m^2/g units. Then by easy algebra, we can get S_p (in $\mu\mathrm{m}^{-1}$ units) as:

$$S_p = S_g \left(\frac{1-\Phi}{\Phi}\right) \rho_g \tag{48}$$

(see [29]), where the grain density is $\rho_g = 2.71\,\mathrm{g/cm}^3$ for calcite, $\rho_g = 2.62\,\mathrm{g/cm}^3$ for quartz.

A different approach is also possible. That would be to consider the thickness δ in Eqs. (35, 47) as a *fitting parameter*, and determine it from cases where *both* the BET specific surface S_g *and* the permeability of the sample k are known from independent laboratory measurements. Then for other rock samples (of the same formation and lithology), this fitting δ-value could be used in Eq. (47).

5 Some Aspects of Triple Porosity

In this section, I propose a new technique, based on microscopy, on how to estimate the transfer factors between pore–pore, pore–fracture, fracture–fracture, vug-fracture, etc. needed for the equations of hydraulic flow in triple-porosity carbonates. As a first step of an ongoing research to generalize the Lorenz curve and Lorenz coefficient (see, e.g., [80]) for heterogeneity estimation in triple-porosity rocks, in Sect. 5.5, I shall generalize the concept of *storativity* for triple-porosity carbonates.

5.1 Neighbor Statistics from Image

Denote by P, F, V the respective sets of the three different types of void such as pore, fracture, and vug which can be distinguished on the microscopic image based on the object's eccentricity, aspect ratio or some other criteria. Define a threshold distance $k \geq 0$ in pixel units and call two objects A and B *neighbors* if their distance satisfies $\mathrm{dist}(A, B) \leq k$. Write a program to find the number of the following neighbors in the image (where # means "number of")

$$N_{pp} = \#\{p_1 \in P, p_2 \in P | \mathrm{dist}(p_1, p_2) \leq k\} \tag{49a}$$

$$N_{vv} = \#\{v_1 \in V, v_2 \in V | \mathrm{dist}(v_1, v_2) \leq k\} \tag{49b}$$

$$N_{ff} = \#\{f_1 \in F, f_2 \in F | \mathrm{dist}(f_1, f_2) \leq k\} \tag{49c}$$

$$N_{pv} = \#\{p \in P, v \in V | \mathrm{dist}(p, v) \leq k\} \tag{49d}$$

$$N_{pf} = \#\{p \in P, f \in F | \mathrm{dist}(p, f) \leq k\} \tag{49e}$$

$$N_{vf} = \#\{v \in V, f \in F | \mathrm{dist}(v, f) \leq k\} \tag{49f}$$

Note the symmetry, e.g., $N_{pf} = N_{fp}$.

Let $N_{\mathrm{neighbors}} = N_{pp} + N_{vv} + N_{ff} + N_{fv} + N_{pf} + N_{vf}$, then one can define the *normalized fractions of different kinds of neighbors* as

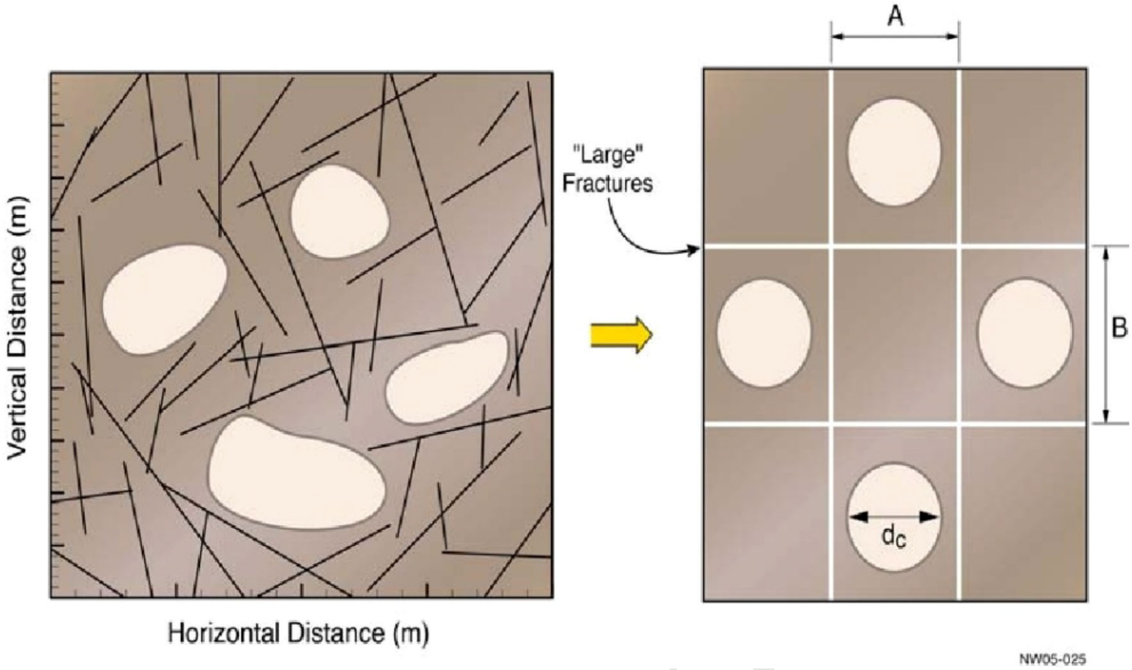

Fig. 7 Triple-porosity rock model where the vugs are connected to fractures through the rock matrix (from [56])

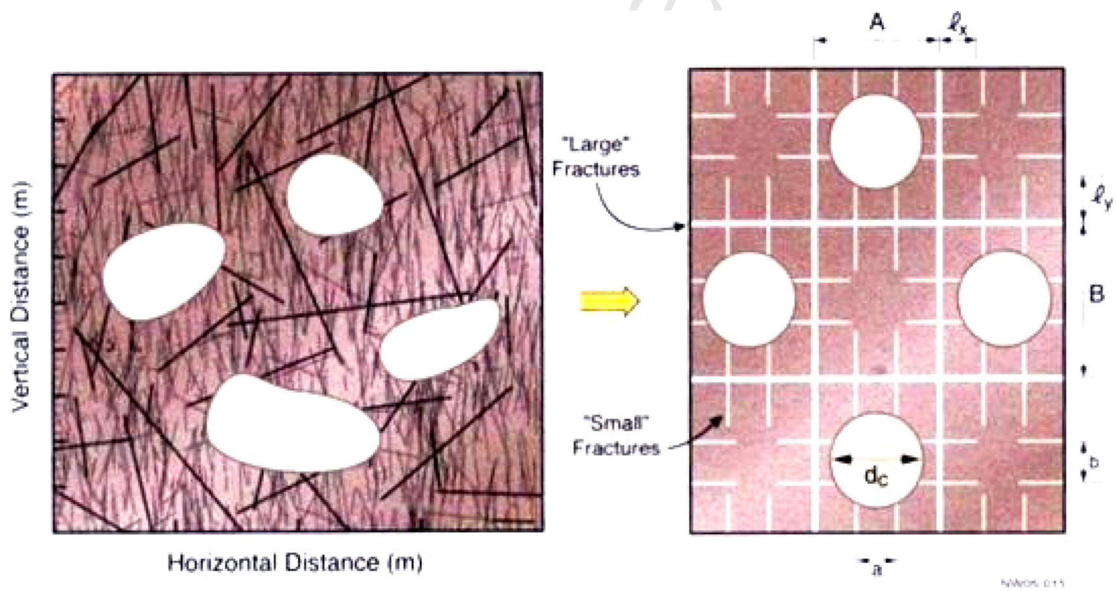

Fig. 8 Triple-porosity rock model where the vugs are connected to main fractures through smaller fractures (from [56])

$$N^*_{ff} = \frac{N_{PP}}{N_{\text{neighbors}}}$$
$$\vdots \qquad (51\ \text{a–f})$$
$$N^*_{vf} = \frac{N_{VF}}{N_{\text{neighbors}}}$$

If there are too many objects in the image then, by the De Lesse principle [32,52] and assuming isotropy, one can estimate the relative fractions of different kinds of neighbors (instead of from the whole image) along a reasonable number, say 50 or 100, of random horizontal or vertical lines.

5.2 The Transfer Factors λ_{mf}, λ_{vf}, λ_{mv} in the Flow Equations

The following ideas of [56–59] can be used to generalize the Warren–Root [60] *dual-porosity* flow model to *triple porosity*. Letting the subscripts f, v, m refer to fracture, vug and

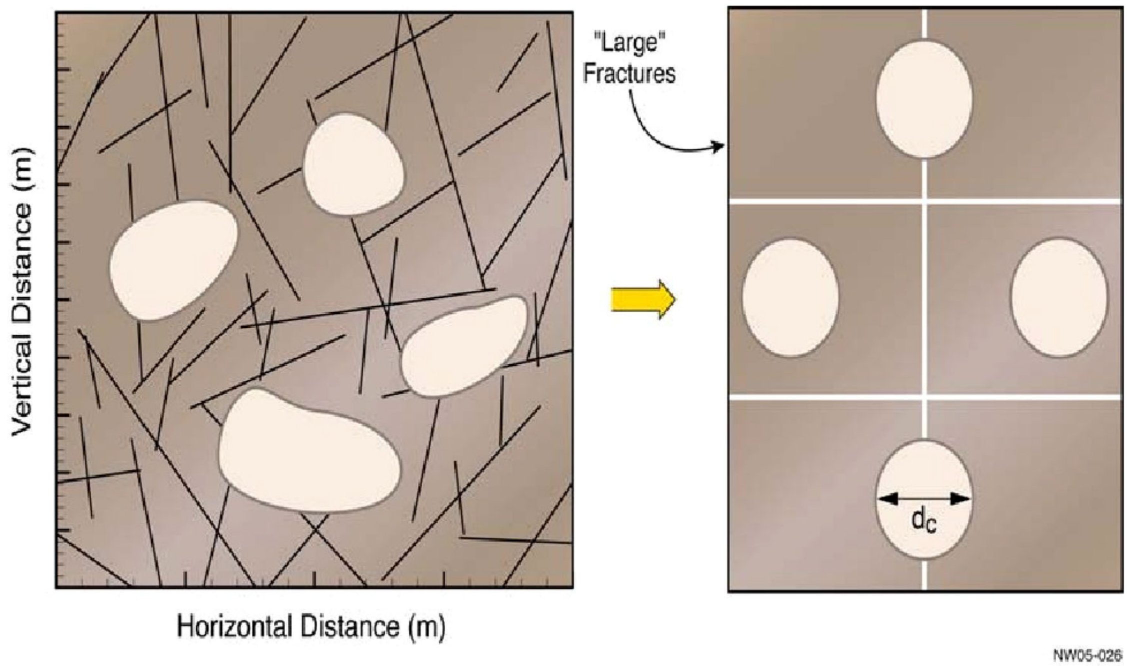

Fig. 9 Triple-porosity rock model where some isolated vugs are connected to fractures through the rock matrix, some are intersected by fractures (from [56])

matrix, respectively, these models assume (1) radial flow into the reservoir of uniform thickness where only fractures feed the well; (2) spatially/temporally constant rock properties; (3) isothermal single-phase compressible fluid with constant viscosity.

The three basic Darcy equations for flow are, in cylindrical geometry:

Flow through the large fractures:

$$\frac{k_f}{\mu}\frac{1}{r}\left(r\frac{\partial P_f}{\partial r}\right) - \Phi_m C_m \frac{\partial P_m}{\partial t} - \Phi_v C_V \frac{\partial P_v}{\partial t} = \Phi_f C_f \frac{\partial P_F}{\partial t} \tag{52}$$

Flow interacting with vugs:

$$\Phi_v C_V \frac{\partial P_v}{\partial t} = \frac{\alpha_{fv} k_v}{\mu}\left(P_f - P_v\right) + \frac{\alpha_{vm} k_m}{\mu}\left(P_m - P_v\right) \tag{53}$$

Flow interacting with matrix:

$$\Phi_m C_m \frac{\partial P_m}{\partial t} = \frac{\alpha_{fm} k_m}{\mu}\left(P_f - P_m\right) + \frac{\alpha_{vm} k_m}{\mu}\left(P_v - P_m\right) \tag{54}$$

In Eqs. (52–54), the coefficients $\alpha_{fv}, \alpha_{fm}, \alpha_{vm}$ are called *interporosity flow shape factors,* k_f, k_v, k_m are the three different permeabilities (assuming isotropy and single-phase flow).

5.3 Interporosity Flow Shape Factors and Their Determination

Consider three distinct cases for the relative position of vugs and fractures (Figs. 7–9 and Table 4, from [56]).

Determination of the inter-porosity flow shape factors from the image:

$$\alpha_{fm} = \frac{A_{fm}}{l_{fm}} \tag{55}$$

where A_{fm} is the total fracture/matrix *connection area* per unit volume of the rock $\left(\mathrm{m}^2/\mathrm{m}^3\right)$, l_{fm} is a characteristic distance (See Table 4). As always done in integral geometry and stereology, A_{fm} is estimated from the 2D microscopic image as *total length of the fracture/matrix common boundary* per unit area of the rock $\left(m/m^2\right)$. The precision of measuring the "common boundary" on the image depends on the way of thresholding, on the pixel size, on the resolution of the microscope and even on the dye used, and apparently has not been studied as yet.

Similarly

$$\alpha_{fv} = \frac{A_{fv}}{l_{fv}} \tag{56}$$

where A_{fv} is the total fracture/vug *connection area* per unit volume of the rock $\left(m^2/m^3\right)$, l_{fv} is a characteristic distance

(See Table 4);

$$\alpha_{vm} = \frac{A_{vm}}{l_{vm}} \tag{57}$$

where A_{vm} is the vug/matrix *connection area* per unit volume of the rock $\left(m^2/m^3\right)$, l_{vm} is is a characteristic distance (see Table 4).

5.4 Flow Equations in Dimensionless Coordinates

Introducing *dimensionless pressure*, *dimensionless radial distance* and *dimensionless time* [59] as:

$$r_D = \frac{r}{r_W}; \tag{58}$$

$$t_D = \frac{t}{\mu r_w^2 \left(\Phi_f C_f + \Phi_v C_v + \Phi_m C_m\right) / k_f} \tag{59}$$

$$P_D\left(r_D; t_D\right) = \frac{2\pi k_f h}{\mu q}\left(P_i - P(r,t)\right); \tag{60}$$

(where r_w is well radius; h reservoir thickness; q flow rate), the flow equations (52–54) reduce to

$$\omega_f \frac{\partial P_{Df}}{\partial t_D} - \frac{1}{r_D}\frac{\partial}{\partial r_D}\left(r_D \frac{\partial P_{Df}}{\partial r_D}\right) - \lambda_{fv}\left(P_{Dv} - P_{Df}\right) - \lambda_{fm}\left(P_{Dm} - P_{Df}\right) = 0 \tag{61}$$

$$\omega_v \frac{\partial P_{Dv}}{\partial t_D} + \lambda_{fv}\left(P_{Dv} - P_{Df}\right) + \lambda_{vm}\left(P_{Dv} - P_{Dm}\right) = 0 \tag{62}$$

$$\omega_m \frac{\partial P_{Dm}}{\partial t_D} + \lambda_{fm}\left(P_{Dm} - P_{Df}\right) + \lambda_{vm}\left(P_{Dm} - P_{Dv}\right) = 0 \tag{63}$$

The *inter-porosity transfer parameters* $\lambda_{fv}, \lambda_{fm}, \lambda_{vm}$ and the previously discussed *inter-porosity flow shape factors* $\alpha_{fv}, \alpha_{fm}, \alpha_{vm}$ are related as [59]:

$$\lambda_{fm} = \frac{\alpha_{fm} r_w^2 k_m}{k_f}; \tag{64a}$$

$$\lambda_{fv} = \frac{\alpha_{fv} r_w^2 k_v}{k_f}; \tag{64b}$$

$$\lambda_{vm} = \frac{\alpha_{vm} r_w^2 k_m}{k_f} \tag{64c}$$

5.5 Storativity in Triple-Porosity Rocks

In the previous Eqs. (61–63), the coefficients ω are called *storativities*. (Recall, that in hydrogeology, *storativity* is the amount of water that an aquifer yields to wells due to the compression of the aquifer.) In triple-porosity rocks, three kinds of storativity should be defined, they add together to 1:

$$\omega_f = \frac{\Phi_f C_f}{\Phi_m C_m + \Phi_f C_f + \Phi_v C_v} \tag{65a}$$

$$\omega_v = \frac{\Phi_v C_v}{\Phi_m C_m + \Phi_f C_f + \Phi_v C_v} \tag{65b}$$

$$\omega_m = \frac{\Phi_m C_m}{\Phi_m C_m + \Phi_f C_f + \Phi_v C_v} \tag{65c}$$

where the indices f, v, m refer to fracture, vug and matrix porosity. C_m, C_v, C_f are the compressibilities of the formation containing only one special type of pore. Here

$$\Phi_m, \Phi_v, \Phi_f, \text{ with } \Phi_m + \Phi_v + \Phi_f = 1 \tag{66}$$

are the three kind of porosities. By the De Lesse principle [32,52], the three porosities Φ_m, Φ_v, Φ_f can be estimated from microscopy if we have some tools of image processing distinguishing between these different objects (such as the eccentricity or aspect ratio of the pore shape, some other ideas are pursued in our recent study [21]). If the three compressibilities are known, then $\omega_m, \omega_v, \omega_f$ can be computed from Φ_m, Φ_v, Φ_f and C_m, C_v, C_f. If the compressibilities are not given, one has to assume $C_m = C_v = C_f$ and then storativities become the same as the porosities.

6 ACF (Autocorrelation Function)-Based Techniques for Permeability

6.1 ACF of a Binary Image

The binary image (what we get after thresholding) was represented earlier as

$$F(x,y) = \begin{cases} 1 & \text{if } (x,y) \in \Pi \\ 0 & \text{if } (x,y) \notin \Pi \end{cases} \tag{67}$$

where Π denotes the "foreground," i.e., the total set of pores in the microscopic image of the rock. In mathematical terms, $F(x,y)$ is the *characteristic function* of the pores. Assume that $F(x,y)$ is a translation invariant and isotropic *random field* [69,70]. Denoting by Φ the overall porosity, because of translation invariance a randomly selected point (x,y) is with probability Φ in pore, with probability $1-\Phi$ in the rock matrix. Denoting with angular brackets $\langle\cdots\rangle$ expected values over different realizations of the random field, the mean and variance of $F(x,y)$ are

$$\langle F(x,y)\rangle = \Phi \cdot 1 + (1-\Phi)\cdot 0 = \Phi \tag{68}$$

$$\left\langle [F(x,y) - \Phi]^2 \right\rangle = \left\langle F^2(x,y) - 2\Phi F(x,y) + \Phi^2 \right\rangle = \Phi - \Phi^2 = \Phi(1-\Phi) \tag{69}$$

In case of translation and rotation invariance of $F(x,y)$, the normalized *autocorrelation Function* (ACF, first intro-

Journal: 13369 MS: 2138 TYPESET DISK LE CP Disp.:2016/4/13 Pages: 21 Layout: Large

duced to Earth Sciences by Scheidegger [61,62]) of $F(x, y)$, defined as $\frac{\langle [F(x,y)-\Phi][F(x+\xi,y+\eta)-\Phi]\rangle}{\langle [F(x,y)-\Phi]^2\rangle}$, only depends on the distance between (x, y) and $(x + \xi, y + \eta)$ that is on $\rho = \sqrt{\xi^2 + \eta^2}$, so that it can be written in the form

$$\begin{aligned}
&\frac{\langle [F(x, y) - \Phi] \cdot [F(x + \xi, y + \eta) - \Phi]\rangle}{\langle [F(x, y) - \Phi]^2\rangle} \\
&\quad = \frac{\langle [F(x, y) - \Phi] \cdot [F(x + \xi, y + \eta) - \Phi]\rangle}{\Phi(1 - \Phi)} \\
&\quad = R_{FF}(\rho). \qquad (70)
\end{aligned}$$

Berryman and Blair [63] have made more precise the arguments of the classic paper of Debye et al. [51] (what we used previously to derive Eq. 41) and proved that the specific surface area of the pore boundaries can be estimated from the slope of the ACF at $\rho = 0$ as

$$S_p = -4 \frac{\mathrm{d}}{\mathrm{d}\rho} R(\rho)\bigg|_{\rho=0}, \qquad (71)$$

an equation which, when substituted into the Kozeny–Carman Eq. (17) (and assuming some reasonable default values for shape factor b and tortuosity τ), can be used to predict permeability *from the autocorrelation analysis of the microscopic image*. Similarly, if we have already established a calibration $S_{wi} = \lambda S_p$, we can also use Timur's (or Timur-type) equations to predict permeability from the image's ACF.

If the characteristic function $F(x, y)$ of the pore space has an exponential ACF with correlation distance ρ_0, i.e., if

$$R(\rho) = \exp\left[-\frac{\rho}{\rho_0}\right], \qquad (72)$$

then Eq. 71 gives $S_{\text{spec}} = \frac{4}{\rho_0}$ and using this in the KC (Eq. 17) gives

$$k = \text{const} \cdot \Phi^3 \rho_0^2 \qquad (73)$$

which is not only *dimensionally correct* (because permeability has the dimension *distance*^{2}) but also seems physically reasonable, because on the right-hand side (RHS) the "ρ_0" is of the order of pore size, i.e., it has a similarly huge dynamic range in sedimentary rocks as the permeability k itself has.

Berryman and Blair's paper [63] has attracted many follow-ups which attempted, with varying success, to predict permeability from microscopy. A notable, much cited paper on the tracks of [63] was Ioannidis et al. [64] and its very nice experimental verification 4 years later by a Colombian researcher [65].

Ioannidis et al. [64] observed that the exponential ACF, $R(\rho) = \exp\left[-\frac{\rho}{\rho_0}\right]$, though frequently reported for ordinary black-and-white photographs, is not applicable for microscopic images of sedimentary rock, where a *stretched exponential* function [66] better describes the experimentally obtained ACF. Using the notation of [64], this ACF is

$$R(u) = \exp\left[-\left(\frac{u}{\lambda}\right)^n\right] \qquad (74)$$

where λ is the correlation distance, n is a positive real exponent.

The derivative of this ACF at $u = 0$ is $\frac{\mathrm{d}}{\mathrm{d}u} R(u)\Big|_{u=0} = -\frac{n}{\lambda^n} u^{n-1}\Big|_{u=0}$ which, except for $n = 1$, cannot express the specific surface area by means of Eq. (71) because for $n < 1$ the RHS is divergent, while for $n > 1$ the RHS is zero. To avoid this difficulty, Ioannidis et al. [64] recommended to use an *average correlation distance*

$$I_S = \int_0^\infty R(u)\mathrm{d}u = \int_0^\infty \exp\left[-\left(\frac{u}{\lambda}\right)^n\right] \mathrm{d}u \qquad (75)$$

With the substitution $x = \left(\frac{u}{\lambda}\right)^n$ and recalling the definition of the Gamma function $\Gamma(z) = \int_0^\infty t^{z-1} \mathrm{e}^{-t} \mathrm{d}t$ we find

$$I_S = \int_0^\infty \exp\left[-\left(\frac{u}{\lambda}\right)^n\right] \mathrm{d}u = \frac{\lambda}{n} \Gamma\left(\frac{1}{n}\right) \qquad (76)$$

(tabulated integral 3.478 in [67]). If for a given rock type n is not varying in a wide range, in Eq. (76) the changes in the expression $\frac{1}{n}\Gamma\left(\frac{1}{n}\right)$ are not too significant and the scaling rule $k = \text{const} \cdot \Phi^3 \rho_0^2$ (Eq. 73) that was valid for the exponential ACF, $R(\rho) = \exp\left[-\frac{\rho}{\rho_0}\right]$, would be, more generally

$$k \propto \Phi^\alpha I_s^\beta \qquad (77)$$

(see 64, *Abstract*), or:

$$\ln k = a + b \ln \Phi + c \ln I_S, \qquad (78)$$

(64, Eq. 6; or 65, Eq. 2.)

A similar empirical equation to connect permeability with image ACF was suggested by Coskun and Wardlaw [68], but instead of the average correlation distance I_S they used the characteristic *porel* size (porel = "porosity element").

Ioannidis et al. [64] used backscatter SEM images (about 60 images per sample) of thin sections from 15 Canadian rock samples of different lithology, and found λ, n and I_S and the following fitting parameters to Eq. (78): $a = 9.3252$; $b = 5.750$; $c = 1.572$ (see Table 5). The only cases when the fit did not work satisfactorily were *samples with low porosity but high permeability* (see Table 5, Gilwood sandstone #7, $\Phi = 0.134$, $k = 412$ mD, possible reason: existence of small fractures not affecting porosity), or *samples with high porosity and low permeability* (see Table 5, Viking sandstone

Journal: 13369 MS: 2138 ☐ TYPESET ☐ DISK ☐ LE ☐ CP Disp.:2016/4/13 Pages: 21 Layout: Large

Table 5 Data from [64], fitting parameters to Eq. 78: $a = 9.3252$; $b = 5.750$; $c = 1.572$

Lithology	Sample	Φ (optical)	Φ (core)	k (mD)	λ (micron)	n	I_S(micron)
Pekisko dolomite (256 images)	58A	0.204	0.197	728.0	49.36	0.734	59.85
	45A	0.149	0.153	25.9	18.11	0.681	23.55
	45B	0.130	0.129	28.0	23,30	0.704	29.34
	35B	0.109	0.101	3.5	24.81	0.556	41.54
Montney dolomitic limestone (263 images)	9B	0.119	0.152	5.3	6.89	0.834	7.59
	31B	0.125	0.129	1.8	6.41	0.750	7.63
	30B	0.125	0.122	2.1	6.50	0.766	7.61
	31A	0.109	0.102	0.5	5.25	0.736	6.35
Gilwood sandstone (227 images)	16	0.192	0.202	646.0	40.19	0.801	45.49
	15A	0.168	0.173	114.0	28.49	0.689	36.62
	7	0.129	0.134	412.0	38.69	0.840	42.41
	4B	0.113	0.069	1.7	44.32	0.635	62.18
Viking sandstone (145 images)	4A	0.197	0.198	6.5	18.48	0.758	21.83
	1	0.117	0.125	3.0	25.33	0.833	27.92
Fahler sandstone (30 images)	13F	0.077	0.113	4.4	12.21	0.729	14.89

#4A, $\Phi = 0.197$, $k = 6.5$ mD, possible reason: diagenetic clay blocking the throats, see [14]).

6.2 Permeability from Unbinarized Rock Image?

To find the value of $I_S = \frac{\lambda}{n}\Gamma\left(\frac{1}{n}\right)$, one needs good estimates of the correlation distance λ and of the stretching exponent "n" in Eq. (74). To get λ and n, a precise estimation of the ACF, $\frac{\langle[F(x,y)-\Phi]\cdot[F(x+\xi,y+\eta)-\Phi]\rangle}{\Phi(1-\Phi)} = R(\rho)$ is needed. A careful reading of [64,65] reveals that the biggest problem is the proper *thresholding* of the images, otherwise the small pore throats (which have an enormous significance in fluid flow) would be missed, and so could not contribute to the estimated ACF. As a final part of this Review, I propose a new way of *using the original full-dynamic range image to compute the ACF.* The estimation of porosity Φ is also not without problems, and strongly depends on thresholding, but it has smaller significance on the estimated k than the errors in n and λ and consequently on the integral I_S. Comparing the 2nd and 3rd columns of Table 5 (taken from [64]) shows that with careful measurements and good binarization, the optical porosity and core porosity do not deviate significantly.

6.2.1 Permeability from Rock Image Using Simulated Probing by EM Waves

To present the idea, we need to introduce the theory of *fluctuations of waves* propagating in isotropic, randomly heterogeneous media, and the *(transverse)* correlation of these fluctuations. We shall follow the classic treatment of Chernov [69].

6.2.1.1 Amplitude Fluctuations of Waves Propagating in Heterogeneous Media and their Transverse Correlation

Consider an acoustic or electromagnetic (EM) wave propagating in a randomly heterogeneous medium [69–71], assume that the propagation velocity in the medium is randomly fluctuating around a constant value C_0 as

$$C(x, y) = \frac{C_0}{1 + \delta(x, y)} \tag{79}$$

where, in case of isotropy,

$$\begin{aligned} &\langle\delta(x, y)\rangle = 0; \ \left\langle\delta^2(x, y)\right\rangle = \delta^2 \ll 1; \\ &R_{CC}(r) = \langle C(x, y) \cdot C(x + r\cos\varphi, y + r\sin\varphi)\rangle \\ &\qquad = \delta^2 \exp(-r/r_0), \end{aligned} \tag{80}$$

where r_0 is the correlation distance of inhomogeneities. Expected values are taken over all realizations of the random field $\delta(x, y)$. Then the mean transit time fluctuations $\langle(\Delta t)^2\rangle$and mean logarithmic amplitude fluctuations $\left\langle\left(\Delta \ln \frac{|A|}{|A_0|}\right)^2\right\rangle$grow with distance L as

$$\left\langle(\Delta t)^2\right\rangle = \frac{L}{C_0^2}\left\langle\delta^2\right\rangle r_0\sqrt{\pi} \tag{81}$$

$$\left\langle\left(\Delta \ln \frac{|A|}{|A_0|}\right)^2\right\rangle = gL \tag{82}$$

It is assumed that the correlation length r_0 is much larger than the mean wavelength (case of geometrical optics). In Eq. (82) the factor g is the so-called *turbidity factor*, and it has such a complicated dependence on wavelength and on correlation length r_0 [71,72, fortheacousticcase] that it cannot be used for the estimation of r_0 from the measured amplitude fluctuations $\left\langle\left(\Delta \ln \frac{|A|}{|A_0|}\right)^2\right\rangle$. I propose an alternative way based on the important discovery of Chernov [69, pp.95–110], according to which *the transverse (*i.e., *perpendicular to the direction of the wave propagation) ACF of the amplitudes (*i.e., *of the absolute amplitudes* $|A|$, *not logarithmic amplitudes as in Eq. 82) has the same correlation distance as the inhomogeneities of the medium where the wave propagates. As work hypothesis I assume that the amplitudes of simulated EM waves propagating through the optical image of the medium will have a similar ACF to that of the medium itself, so that its transverse ACF can be used as a proxy instead of the ACF of the image*. The transmitted wave can be computed by any numerical solver of the EM wave propagation, for example by the MAXWELL program [73–75]. The physical property ("dielectric constant") controlling wave speed, reflection and transmission coefficients should be assigned to each pixel of the image, depending on the gray scale of the pixel values, using a linear or nonlinear (as e.g., "Pareto," i.e., power function like) correspondence between gray scales and dielectric constants.

6.3 Comparison of Two Approaches

The ACF of the microscopic image can be computed in two different ways (from binarized, or from the original images). From the ACF then one must find λ and n, determine I_S and find the fitting parameters a, b, c to express the permeability k measured on the given core, using Eq. (78). In the two approaches, the ACF is computed, in turn, (a) from the binary (1 = pore, 0 = rock matrix) image or (b) from the non-binarized full-dynamic range image. Computationally, the approach (b) is done by finding the correlation distance by transforming gray scales to dielectric constants, probing the image with simulated EM waves, and determining their transverse correlation. This is an ongoing research of the author, with no experimental evidence as yet.

7 Conclusions and Outlook

The motivation of this Review has been my firm belief that the recent DRP (Digital Rock Physics) revolution [4–9] promising to find macroscopic bulk properties from 3D microscanned images of small pieces of rock still has not made superfluous the search for simple rock models and techniques based on 2D rock images. In a sense, this Review is sequel to [76], where a simple geometric rock model connected transfer and elastic properties in sedimentary rocks. (When writing [76], I did all computations on a handheld calculator, while DRP problems solved with Lattice Boltzman Models need high-performance computers, [77].) The search for rock models, started in [76], is still ongoing in the direction of triple porosity. Another novel technique, sliding-window entropy filtering [21], that has been briefly mentioned, seems to have exciting properties to discriminate between different pore types in triple-porosity rocks, so that it might help in finding the neighborhood probabilities and transfer factors described in Sect. 5. The powerful *method of moments* (Sect. 2.2) has only been referred to in connection with tortuosity (Sects. 3.3.2.1–3.3.2.3); I envisage it will also find future applications in triple-porosity studies because the eccentricity and aspect ratio computed from the moments can distinguish between different pore types. The tortuosity estimate, based on the method of moments and discussed in Sect. 3.3.2.1, leads to a direction-dependent (i.e., possibly anisotropic) permeability, as briefly mentioned (around the end of Sect. 3.3.2.2). Autocorrelation or the related semivariogram techniques have already been generalized to the anisotropic case both in random wave theory and geostatistics [69,80], that is in principle they might be used to predict anisotropic permeability from an anisotropic image, but I could not find any published study on this. As discussed in

Section 6.1, there are cases both in sandstones and carbonates when permeability could not be predicted from microscopy in any routine way (existence of small fractures not affecting porosity but increasing permeability, or diagenetic clay blocking the throats, see samples 7 and #4A in Table 5). In the most influential permeability study of the last two decades, Amaefule et al. [25] documented strong correlation between FZI (Flow Zone Indicator) and rock-textural properties such as specific surface area and grain size distribution. These ideas have not been followed up yet as much as they deserve, and I still envisage that—in light of the revival of the Flow Unit concept as "GHE" (Global Hydraulic Element, [26])—the image analysis of micrographs will be included again in the toolbox of petrophysicists.

8 Subjective Notes and Acknowledgments

My interest, early in my career, to study the ACF (autocorrelation function) of binary rock images following up Scheidegger [61,62], has led me first to sound absorption [70,71,78], then to EM wave scattering in geologic materials [73–75]. In the last 25 years, starting with my paper [14], I have become attracted to the intricacies of porosity permeability, and how to understand their relation from the rock image. I acknowledge my indebtedness to all my friends and colleagues who joined me along parts of this tortuous journey, most of all to Prof. Klaudia Oleschko (UNAM, Mexico), Dr. Nabil Akbar (formerly with Saudi Aramco), and Dr. Abdulazeez Abdulraheem (KFUPM).

The phrase "Review of a Dream" in the title is borrowed from the paper [79] (of Guéguen et al., "Upscaling: Effective medium theory, numerical methods and the fractal dream")—a recommended collateral reading for anybody doing rock physics from rock image.

My thoughts on permeability prediction have crystallized through the last 15 years, and some ideas described here have been developed in previous projects financed by Saudi and Mexican Institutions. I would especially like to acknowledge the most recent support provided by King Abdulaziz City for Science and Technology (KACST) through the Science and Technology Unit at King Fahd University of Petroleum and Minerals (KFUPM) for funding my work on the triple-porosity parts of this paper through project No. 11-OIL2144-04, as part of the National Science, Technology and Innovation Plan. Thanks are due to the King Fahd University for the excellent facilities and creative atmosphere. Last but not least, thanks are due to Professor Bassam El-Ali, Managing Editor of AJSE for kindly inviting me to write this Review paper for his prestigious Journal.

References

1. Carman, P.C.: Flow of Gases Through Porous Media. Butterworth, London (1956)
2. Timur, A.: An investigation of permeability, porosity, and residual water saturation relationships. SPWLA 9th Annual Logging Symp., June 23–28, 1968 (1968a)
3. Timur, A.: An investigation of permeability, porosity, and residual water saturation relationships for sandstone reservoirs. Log Anal. **9**(4), 8–17 (1968)
4. Andrä, H.; Combaret, N.; Dvorkin, J.; Glatt, E.; Han, J.; Kabel, M.; Keehm, Y.; Krzikalla, F.; Lee, M.; Madonna, C.; Marsh, M.; Mukerji, T.; Saenger, E.H.; Sain, R.; Saxena, N.; Ricker, S.; Wiegmann, A.; Zhan, X.: Digital rock physics benchmarks—part I: imaging and segmentation. Comput. Geosci. **50**, 25–32 (2013)
5. Andrä, H.; Combaret, N.; Dvorkin, J.; Glatt, E.; Han, J.; Kabel, M.; Keehm, Y.; Krzikalla, F.; Lee, M.; Madonna, C.; Marsh, M.; Mukerji, T.; Saenger, E.H.; Sain, R.; Saxena, N.; Ricker, S.; Wiegmann, A.; Zhan, X.: Digital rock physics benchmarks—part II: computing effective properties. Comput. Geosci. **50**, 33–43 (2013)
6. Dvorkin, J.; Derzhi, N.; Fang, Q.; Nur, A.; Nur, B.; Grader, A.; Baldwin, C.; Tono, H.; Diaz, E.: From micro to reservoir scale: permeability from digital experiments. Lead. Edge **28**, 1446–1452 (2009)
7. Dvorkin, J.; Derzhi, N.; Diaz, E.; Fang, Q.: Relevance of computational rock physics. Geophysics **76**(5), E141–E153 (2011)
8. Keehm, Y.: Computational rock physics: transport properties in porous media and applications. Ph.D. Thesis, Stanford University (2003)
9. Knackstedt, M.A.; Latham, S.; Madadi, M.; Sheppard, A.; Varslot, T.; Arns, C.: Digital rock physics: 3D imaging of core material and correlations to acoustic and flow properties. Lead. Edge **28**(1), 28–33 (2009)
10. Sorbie, K.S.; Skauge, A.: Can network modeling predict two-phase flow functions?. Petrophysics **53**(6), 401–409 (2012)
11. Touati, M.; Suicmez, S.; Funk, J.; Cinar, Y., Knackstedt, M.: Pore network modeling of Saudi Aramco rocks: a comparative study. SPE Paper 126043 presented at the 2009 SPE Saudi Arabia Section Technical Symposium and Exhibition, Al Khobar, May 2009
12. Zhang, X.; Knackstedt, M.A.: Direct simulation of electrical and hydraulic tortuosity in porous solids. Geophys. Res. Lett. **22**(17), 2333–2336 (1995)
13. Korvin, G.: Fractal Models in the Earth Sciences. Elsevier, Amsterdam (1992)
14. Korvin, G.: A percolation model for the permeability of kaolinite-bearing sandstone. Geophys. Trans. **37**(2–3), 177–209 (1992)
15. Korvin, G.; Mohiuddin, M.A.; Abdulraheem, A.: Experimental investigation of the fractal dimension of the pore surface of sedimentary rocks under pressure. Geophys. Trans. **44**(1), 3–19 (2001)
16. Sezgin, M.; Sankur, B.: Survey over image thresholding techniques and quantitative performance evaluation. J. Electron. Imaging **13**(1), 146–165 (2004)
17. Otsu, N.: A threshold selection method from gray-level histograms. IEEE Trans. Syst. Man Cybern. **SMC-9**(1), 62 (1979)
18. Ji, Y.; Baud, P.; Vajdova, V.; Wong, T.-F.: Characterization of pore geometry of Indiana limestone in relation to mechanical compaction. Oil and Gas Science and Technology—Revue de l'Institut Français du Pétrole (2012). doi:10.2516/ogst/2012051
19. Schindelin, J.; Arganda-Carreras, I.; Frise, E.; Kaynig, V.; Longair, M.; Pietzsch, T. et al.: Fiji: an open-source platform for biological-image analysis. Nat. Methods **9**(7), 676–682 (2012)
20. Freire-Gormaly, M.; Ellis, J.S.; Bazylak, A.; MacLean, H.L.: Comparing thresholding techniques for quantifying the dual porosity of Indiana Limestone and Pink Dolomite. Microporous Mesoporous Mater. **207**, 84–89 (2015)
21. Korvin, G.; Sterligov, B.; Oleschko, K.; Cherkasov, S.: Entropy of shortest distance (ESD) as pore detector and pore-shape classifier. Entropy **15**(6), 2384–2397 (2013)
22. Akhiezer, N.I.: The Classical Moment Problem and Some Related Questions in Analysis. Hafner, New York (1965)
23. Teague, M.R.: Image analysis via the general theory of moments. J. Opt. Soc. Am. **70**(8), 920–930 (1980)
24. Jähne, B.: Digitale Bildverarbeitung, 4th edn. Springer, Berlin (1997)
25. Amaefule, J.O.; Altunbay, M.; Kersey, D.G.; Kelaan, D.K.: Enhanced reservoir description: using core and log data to identify hydraulic (flow) units and predict permeability in uncored intervals/wells. SPE Paper # 26436 (1993)
26. Corbett, P.W.M.; Ellabad, Y.; Mohammed, K.; Posysoev: Global hydraulic elements—elementary petrophysics for reduced reservoir modeling. EAGE 65th Conference, Ext. Abstracts, vol. 1, paper F-26, Stavanger, 2–6 June 2003
27. Railsback, L.B.: An atlas of pressure dissolution features. Lecture Notes, Department of Geology, University of Georgia, Athens, Georgia 30602-2501 USA. http://www.gly.uga.edu/railsback/PDFindex1.html (2002)
28. Mortensen, J.; Engstrøm, F.; Lind, I.: The relation among porosity, permeability, and specific surface of chalk from the Gorm field, Danish North Sea. SPE Reserv. Eval. Eng. **1**, 245–251 (1998)
29. Hossain, Z.; Grattoni, C.A.; Solymar, M.; Fabricius, I.L.: Petrophysical properties of greensand as predicted from NMR measurements. Pet. Geosci. **17**, 111–123 (2011)
30. Mandelbrot, B.: The Fractal Geometry of Nature. W.H. Freeman & Co., New York (1982)
31. Feder, J.: Fractals. Plenum, Plenum Press, New York (1988)
32. Oleschko, K.: Delesse principle and statistical fractal sets: 1. Dimensional equivalents. Soil Tillage Res. **49**, 255 (1988)
33. Koponen, A.; Kataja, M.; Timonen, J.: Tortuous flow in porous media. Phys. Rev. E **54**, 406 (1996)
34. Koponen, A.; Kataja, M.; Timonen, J.: Permeability and effective porosity in porous media. Phys. Rev. E **56**, 3319 (1997)

35. Comiti, J.J.; Renaud, M.: A new model for determining mean structure parameters of fixed beds from pressure drop measurements: application to beds packed with parallelepipedal parcticles. Chem. Eng. Sci. **44**(7), 1539–1545 (1989)
36. Yu, B.-M.: Fractal character for tortuous streamtubes in porous media. Chin. Phys. Lett. **22**(1), 158–160 (2005)
37. Sisavath, S.; Ying, X.D.; Zimmerman, R.W.: Effect of stress on the hydraulic conductivity of rock pores. Phys. Chem. Earth (A) **25**(2), 163–165 (2000)
38. Schlueter, E.M.; Zimmerman, R.W.; Witherspoon, P.A.; Cook, N.G.W.: The fractal dimension of pores in sedimentary rocks and its influence on permeability. Eng. Geol. **48**, 199–215 (1997)
39. Koplik, J.; Lin, C.; Vermette, M.: Conductivity and permeability from microgeometry. J. Appl. Phys. **56**, 3127–3131 (1984)
40. Kilian, J.: Simple image analysis by moments Version 0.2. http://breckon.eu/toby/teaching/dip/opencv/SimpleImageAnalysisbyMoments.pdf (2001)
41. Takahashi, M.; Ahn, C.; Kato, M.: Hydraulic stress effect on 3-dimensional pore network and permeability change. In: Quian, Q., Zhou, Y. (eds.) Harmonising Rock Engineering and the Environment. 12th ISRM Int'l. Congress on Rock Mechanics, pp. 542–546 Taylor & Francis Group, London (2012)
42. Zhang, Z.F.; Ward, A.L.; Gee, G.W.: A tensorial connectivity–tortuosity concept to describe the unsaturated hydraulic properties of anisotropic soils. Vadose Zone J. **2**(3), 313–321 (2003)
43. Peters, E.J.: Advanced Petrophysics, vol 1. Live Oak Book Company, Austin, TX (2012)
44. Schlumberger Well Surveying Co., Log Interpretation Chart Book. (1962)
45. Glover P.W.J.: BP, ARCO Lecturer in Petrophysics, The Petrophysics MSc Course Notes. University of Aberdeen, Department of Geology and Petroleum Geology (2012)
46. Wyllie, M.R.J.; Rose, W.D.: Some theoretical considerations related to the quantitative evaluation of the physical characteristics of reservoir rock from electrical log data. Pet. Trans. AIME **189**, 105 (1950)
47. Morris, R.L.; Biggs, W.P.: Using log-derived values of wáter saturation and porosity. Trans. of SPWLA 8th Annual Logging Symp., Paper X, 26pp (1967)
48. Torskaya, T.; Jin, G.; Torres-Verdin, C.: Pore-level analysis of the relationship between porosity, irreducible water saturation, and permeability of clastic rocks. SPE# 109878 (2007)
49. Tixier, M.P.: Evaluation of permeability from electric-log resistivity gradients. Oil Gas J. (1949)
50. Ahmed, U.; Crary, S.F.; Coates, G.R.: Permeability estimation: the various sources and their interrelationships. J. Pet. Technol. **43**(5), 578–587 (1991)
51. Debye, P.; Anderson, H.R.; Brumberger, H.: Scattering by an inhomogeneous solid. II. The correlation function and its application. J. Appl. Phys. **28**(6), 679–683 (1957)
52. Kim, T.W.; Tokunaga, T.K.; Shuman, D.B.; Sutton, S.R.; Newville, M.; Lanzirotti, A.: Thickness measurements of nanoscale brine films on silica surfaces under geologic CO2 sequestration conditions using synchrotron X-ray fluorescence. Water Resour. Res. **48**, 1–13 (2012)
53. Adams, T.; Grant, C.; Watson, H.: A simple algorithm to relate measured surface roughness to equivalent sand-grain roughness. Int. J. Mech. Eng. Mechatron. **1**(1), 66–71 (2012)
54. Brunauer, S.; Emmett, P.H.; Teller, E.: Adsorption of gases in multimolecular layers. J. Am. Chem. Soc. **60**, 309–319 (1938)
55. Mayhew, T.M.; Cruz-Olive, L.-M.: Caveat on the use of the Delesse principle of areal analysis for estimating component volume densities. J. Microsc. **102**(2), 195–207 (1974)
56. Kang, Z.; Wu, Y.S.; Li, J.; Wu, Y.; Zhang, J.; Wang, G.: Modeling multiphase flow in naturally fractured vuggy petroleum reservoirs. SPE 102356, San Antonio, Texas, 24–27 Sept 2006
57. Lim, K.T.; Aziz, K.: Matrix-fracture transfer shape factors for dual-porosity simulators. J. Pet. Sci. Eng. **13**, 169–178 (1995)
58. Wu, Y.-S.; Qin, G.; Ewing, R.E.; Efendiev, Y.; Kang, Z.; Ren, Y.: A multiple-continuum approach for modeling multiphase flow in naturally fractured vuggy petroleum reservoirs. SPE 104173, Beijing China, 5–7 Dec 2006
59. Wu, Y.-S.; Ehlig-Economides, C.; Qin, G.; Kang, Z.; Zhang, W.; Ajayi, B.; Tao, Q.: A triple-continuum pressure transient model for a naturally fractured vuggy reservoir. Lawrence Berkeley Natl. Lab. Report. 08-28-2007, http://escholarship.org/uc/item/8fr0m0pp
60. Warren, J.E.; Root, P.J.: The behavior of naturally fractured reservoirs. Soc. Pet. Eng. J. **3**(3), 245–265 (1963)
61. Scheidegger, A.E.: The Physics of Flow Through Porous Media, 2nd edn. University of Toronto Press, Toronto (1960)
62. Fara, H.D.; Scheidegger, A.E.: Statistical geometry of porous media. J. Geophys. Res. **66**(10), 3270–3284 (1961)
63. Berryman, J.G.; Blair, S.C.: Use of digital image analysis to estimate fluid permeability of porous materials. Application of the two-point correlation function. J. Appl. Phys. **60**(6), 1930–1938 (1986)
64. Ioannidis, M.A.; Kwiecien, M.J.; Chatzis, I.F.: Statistical analysis porous microstructure as a method for estimating reservoir permeability. J. Pet. Sci. Eng. **16**, 251–261 (1996)
65. Cobaleda, G.E.: A study of image autocorrelation as a method to characterize porosity and estimate permeability. CT&F—Ciencia, Tecnologia y Futuro, **2**(1): 16 (2000)
66. Johnston, C.: Stretched exponential relaxation arising from a continuous sum of exponential decays. Phys. Rev. B. **74**, 184430 (+ Erratum, Phys. Rev. B. **77**, 179901) (2006 & 2008)
67. Gradshteyn, I.S.; Ryzhik, I.M.; Jeffrey, A.; Zwillinger, D., (eds.): Table of Integrals, Series, and Products, 4th edn. Academic Press, New York (1980)
68. Coskun, S.B.; Wardlow, N.C.: Estimation of permeability from image analysis of reservoir sandstones. J. Pet. Sci. Eng. **10**, 1–16 (1993)
69. Chernov, L.A.: Wave Propagation in a Random Medium. Dover, New York (1960)
70. Korvin, G.: Certain problems of seismic and ultrasonic wave propagation in a medium with inhomogeneities of random distribution. II. Wave attenuation and scattering on random inhomogeneities. Geophys. Trans. **24**(Supplement 2), 3–38 (1977)
71. Korvin, G.: A few unsolved problems of applied geophysics. Geophys. Trans. **31**(4), 373–389 (1985)
72. Sato, H.; Fehler, M.F.: Seismic Wave Propagation and Scattering in the Heterogeneous Earth. Springer, New York (1997)
73. Oleschko, K.; Korvin, G.; Balankin, A.S.; Khachaturov, R.; Flores, D.; Figueroa, B.; Urrutia, F.; Brambila, P.F.: Fractal scattering of microwaves from soils. Phys. Rev. Lett. **89**(18), 1885011–1885014 (2002)
74. Oleschko, K.; Korvin, G.; Figueroa, B.; Vuelvas, M.A.; Balankin, A.S.; Flores, L.; Carreón, D.: Fractal radar scattering from soil. Phys. Rev. Ser. E **13**(041403), 1–13 (2003)
75. Korvin, G.; Khachaturov, R.V.; Oleschko, K.; Ronquillo, G.; Escalante, J.-J.: Computer simulation of microwave propagation in heterogeneous and fractal media. Comput. Geosci. Submitted (2016)
76. Korvin, G.; Oleschko, K.; Abdulraheem, A.: A simple geometric model of sedimentary rock to connect transfer and acoustic properties. Arab. J. Geosci. **7**(3), 1127–1138 (2013)
77. Tölke, J.; Baldwin, C.; Mu, Y.; Derzhi, N.; Fang, Q.; Grader, A.; Dvorkin, J.: Computer simulations of fluid flow in sediment: from images to permeability. Lead. Edge **29**(1), 68–74 (2010)
78. Korvin, G.; Armstrong, B.H.: Frequency-independent background internal friction in heterogeneous solids; discussion and reply. Geophysics **46**, 1314–1315 (1981)

79. Guéguen, Y.; Le Ravalec, M.; Ricard, L.: Upscaling: effective medium theory, numerical methods and the fractal dream. Pure Appl. Geophys. **163**, 1175–1192 (2006)

80. Jensen, L.J.; Lake, W.L.; Patrick Corbett, W.M.; Goggin, J.D.: Statistics for Petroleum Engineers and Geoscientists. Elsevier, Amsterdam (2000)

Journal: **13369** MS: **2138** ☐ TYPESET ☐ DISK ☐ LE ☐ CP Disp.:**2016/4/13** Pages: **21** Layout: **Large**